



**ALTERATION OF THRUST STAND DYNAMICS  
USING HYDRAULIC FORCE FEEDBACK**

**Sam P. Ragsdale  
ARO, Inc.**

**December 1967**

This document has been approved for public release  
and sale; its distribution is unlimited.

PROPERTY OF 3. AIR FORCE  
AEDC LIBRARY  
F40600-69 C-0001/

**ARNOLD ENGINEERING DEVELOPMENT CENTER  
AIR FORCE SYSTEMS COMMAND  
ARNOLD AIR FORCE STATION, TENNESSEE**

# ***NOTICES***

When U. S. Government drawings specifications, or other data are used for any purpose other than a definitely related Government procurement operation, the Government thereby incurs no responsibility nor any obligation whatsoever, and the fact that the Government may have formulated, furnished, or in any way supplied the said drawings, specifications, or other data, is not to be regarded by implication or otherwise, or in any manner licensing the holder or any other person or corporation, or conveying any rights or permission to manufacture, use, or sell any patented invention that may in any way be related thereto.

Qualified users may obtain copies of this report from the Defense Documentation Center.

References to named commercial products in this report are not to be considered in any sense as an endorsement of the product by the United States Air Force or the Government.

ALTERATION OF THRUST STAND DYNAMICS  
USING HYDRAULIC FORCE FEEDBACK

Sam P. Ragsdale  
ARO, Inc.

This document has been approved for public release  
and sale; its distribution is unlimited.

## FOREWORD

The work reported herein was sponsored by the Arnold Engineering Development Center (AEDC), Air Force Systems Command (AFSC), under Program Element 6240518F, Project 5730, and Task 573004.

The results of the test were obtained by ARO, Inc. (a subsidiary of Sverdrup & Parcel and Associates, Inc.), contract operator of the AEDC, AFSC, Arnold Air Force Station, Tennessee, under Contract AF 40(600)-1200. The work was performed from May through August, 1967, under ARO Project No. BC5820, and the manuscript was submitted for publication on October 2, 1967.

This technical report has been reviewed and is approved.

I. F. Flemming  
Flt Lt, RCAF  
Research Division  
Directorate of Plans  
and Technology

Edward R. Feicht  
Colonel, USAF  
Director of Plans  
and Technology

**ABSTRACT**

This report is concerned with the dynamic behavior of a rocket motor and thrust stand combination when restrained by a hydraulic force balance system. The system is analyzed taking into account the nonlinearities caused by limiting flow and fluid compressibility. The analysis is followed by a discussion of the data obtained from an analog simulation of the system. Investigations of the basic stand without the servo are followed by investigations with the servosystem installed for comparison purposes. Both the time and frequency domains are investigated using ramp and sinusoidal forcing functions of thrust. The results of this investigation show that many desirable advantages may be realized using hydraulic force feedback. The control signals may be adjusted to provide zero displacement of the rocket motor position during the steady portion of the firing and at the same time, provide a high degree of damping. Concurrent with these conditions, the acceleration of the rocket motor may be greatly reduced during the firing transient.

## CONTENTS

	<u>Page</u>
ABSTRACT . . . . .	iii
NOMENCLATURE . . . . .	vi
I. INTRODUCTION . . . . .	1
II. GENERAL TECHNICAL CONSIDERATIONS	
2.1 Thrust Stand . . . . .	4
2.2 Performance Goal . . . . .	5
2.3 Hydraulic Servosystem. . . . .	5
III. SYSTEM ANALYSIS AND COMPONENT SELECTION	
3.1 Thrust Butt . . . . .	8
3.2 Engine and Load-Cell Combination . . . . .	9
3.3 Hydraulic Actuator . . . . .	9
3.4 Servovalve and Hydraulic Amplifier . . . . .	13
IV. SIMULATION RESULTS AND DISCUSSION	
4.1 Configuration 1 . . . . .	15
4.2 Configuration 2 . . . . .	18
4.3 Configuration 3 . . . . .	21
V. CONCLUSIONS. . . . .	28
REFERENCES. . . . .	30

## APPENDIXES

I. TIME AND AMPLITUDE SCALING OF SYSTEM EQUATIONS . . . . .	33
II. SIMULATION CIRCUITS . . . . .	37
III. LOW FREQUENCY SHIFT IN THE RESPONSE OF $F_m$ . . . . .	39

## ILLUSTRATIONS

Figure

1. Rocket Thrust Stand with Hydraulic Servo . . . . .	4
2. Block Diagram of Hydraulic Shaker System. . . . .	5
3. Typical Hydraulic Shaker Frequency Response . . . . .	6
4. Response for a Single Constant Load. . . . .	7

<u>Figure</u>	<u>Page</u>
5. Simplified Hydraulic Piston Actuator . . . . .	10
6. Basic Thrust Stand without the Servo Installed . . . . .	15
7. Basic Thrust Stand Response to Varying Rise Times in Applied Thrust . . . . .	16
8. Frequency Response of Basic Thrust Stand . . . . .	17
9. Response in Manual Mode for Step Change in Servo Command Signal with Pilot Valve Damping Set for $\zeta = 0.25$ . . . . .	19
10. Response in Manual Mode for Step Change in Servo Command Signal with Pilot Valve Damping Set for $\zeta = 0.7$ . . . . .	20
11. Response in Thrust Stand with Servo in Manual Mode for Varying Rise Times in Applied Thrust. . . . .	22
12. Frequency Response of Thrust Stand System in the Manual Mode. . . . .	23
13. Response of Thrust Stand for Varying Rise Times in Applied Thrust . . . . .	25
14. Response of Thrust Stand for a 0.01-sec Rise Time Thrust Function . . . . .	26
15. Frequency Response of Thrust Stand System in the Automatic Mode . . . . .	27
16. Response of Thrust Stand in the Automatic Mode to Varying Thrust Levels with 0.01-sec Rise Times . . . . .	29

**NOMENCLATURE**

$A_p$	Area of actuator piston
$C_b, C_m, C_p$	Damping coefficients
$E$	Servoamplifier output voltage
$e$	Voltage signal
$F_b$	Force applied to thrust butt by actuator
$F_m$	Load cell output (force)
$f$	Frequency

$G$	Relative acceleration
$g$	Gravitational acceleration
$K$	Arbitrary constant
$K_b, K_m$	Spring constants
$M_b, M_m, M_p$	Masses
$P_a, P_a', P_o, P_s$	Pressures
$Q$	Transmissibility at resonance
$q$	Volume flow of fluid
$SG$	Specific gravity of hydraulic fluid
$s$	Laplace complex operator
$T_m$	Thrust function (force)
$t$	Time
$V$	Liquid volume of actuator and lines
$W$	Weight of fluid
$\bar{w}$	Specific weight
$x$	Distance
$\beta$	Bulk modulus
$\delta$	Function of two variables
$\xi$	Dimensionless damping ratio
$\pi$	3.14
$\tau$	Time constant
$\Psi$	Function of two variables
$\omega$	Angular frequency, $2\pi f$

## SECTION I INTRODUCTION

The testing of turbojet and ramjet engines under simulated environmental conditions paved the way for similar testing procedures with rocket motors. At the Arnold Engineering Development Center (AEDC), the transition has involved major modifications in test cells along with construction of new ones. Instrumentation needs, data gathering techniques, data reduction, and general operating procedures have been modified and improved to satisfy the requirements of modern testing.

From the standpoint of instrumentation interests, the switch to rocket motor testing can best be described as a shift in emphasis from steady-state to transient phenomena. Jet engines were generally operated at fixed environmental conditions for each data point and ample time was allowed for all transients to die out after reaching the desired condition. As a result, most of the transducers and recording devices were only required to have good static characteristics. The relatively few special tests involving throttle bursts, combustion instabilities, ignition and flameout transients were usually of low frequency content. Although special recorders were frequently used to record these transients, no stringent dynamic requirements were generally imposed on electrical measuring devices.

The criteria governing the design of thrust stands for jet engines were relatively simple. First, the stand was required to hold the engine in place. Secondly, the stand and load-cell combination was designed to have as high a natural frequency as possible. It was assumed that low frequencies (in the flat region of the stand frequency response) would pass through the stand to the load cell with good fidelity. Perhaps the most serious drawback to this approach was that systems of low damping resulted. Noise could easily excite the thrust stand, and this vibration became the disturbance source for instruments mounted on the engine.

Thrust measurements for rocket motors placed new emphasis on thrust stand dynamics. Fast thrust rise and tailoff transients so greatly excited thrust stands that little information concerning true thrust during these transients could be determined. Early analysis techniques involved everything from hand smoothing thrust recordings to the application of band rejection filters. The futility of these methods quickly accentuated the need for more sophisticated approaches.

The near-linear second-order response of most thrust stands provided a basis for study by early investigators (Refs. 1, 2, and 3). Several methods under the general heading of "thrust compensation" were introduced. These techniques were mainly concerned with determining the forcing function (true axial thrust) of a known differential equation. Nonlinearities such as changes in mass caused by burning and nonlinear spring characteristics could be included provided they could be defined. Operational amplifiers were used for computation and/or simulation, and each method could be used on-line if the necessary preparations were made.

The thrust compensation schemes referred to above were concerned with dynamic compensation for axial thrust measurements. The problem of multicomponent thrust measurements is much more complicated since thrust measurements (static and dynamic) in one direction include components of thrust in other directions. If only static measurements of thrust were of interest, these interactions could be decoupled mechanically or by analytical computation schemes provided the stand settled down after the initial thrust rise (Ref. 4).

The axial thrust component is generally much larger than other components. As a result, measurements in the vertical and side directions will contain a higher degree of distortion. Also, dynamic excitation and ringing in the vertical and horizontal planes will generally originate from the axial thrust. For these reasons a high degree of rigidity and near-critical damping in the axial direction is to be desired in order for static resolution schemes to have meaning.

The use of electrodynamic actuators as active force feedback elements to produce artificial damping has been investigated (Refs. 5 and 6). Their excellent frequency response characteristics when used with special driver amplifiers make them well suited for this application. As force actuators in test cell work, however, they are not well suited because of the force limitations, required cooling, and large physical size-to-force ratios.

This report has been prepared to determine the performance that might be expected using a hydraulic servosystem to alter the dynamics of a typical thrust stand. The study involves an analysis leading to a mathematical model of a thrust system and an analog simulation to study its behavior under controlled conditions. So that the investigation will have practical meaning, typical mass, spring, and damping coefficients as experienced with actual thrust systems have been used. The specifications governing the servovalve and piston actuator are typical of some of the best commercially available units.

Three configurations of the thrust stand and control circuitry are considered in the simulation study on performance. Simulation data were collected and are discussed concerning both the time and frequency domains for each configuration. Configuration 1 deals with the basic thrust stand without the servo installed. This system is considered first so that its data can serve as a reference for comparing the data taken for the other configurations. Configuration 2 considers the same thrust stand with the hydraulic servosystem installed. The actuator is mounted on the thrust butt, and the piston pushes against the load cell. The servosystem is operated as a positional servosystem for this configuration to position the piston with respect to the actuator housing. The command signal is furnished by a manual set-point potentiometer. Configuration 3 is identical to Configuration 2 except that the command signal is furnished by live measurements from the load cell and rocket motor.

The first two configurations are mainly concerned with defining the characteristics of the thrust stand and the effect of adding the positional servosystem. Configuration 3 is mainly concerned with the composition and adjustment of the automatic feedback signal to provide the following characteristics: high degree of damping, absolute return of the motor position to zero after the firing transient, low offset of the motor position during the firing transient, and a large reduction of motor acceleration. Visual optimization of these characteristics is accomplished using the repetitive operation feature of a PACE 231R analog computer. Data are presented, compared, and discussed.

## SECTION II GENERAL TECHNICAL CONSIDERATIONS

Before a detailed analysis of a particular force feedback system can be undertaken, it is important that the stand configuration and desired mode of operation be understood. So that this investigation will produce qualitative conclusions concerning the advantages of the method, the stand configuration and its dynamic characteristics should be typical of those now in use. Similar practical consideration should also be given to the hydraulic servomechanism and the measured system variables used to control it.

This section is concerned with a description of the selected thrust stand, its lumped parameter representation, and the desired performance under controlled conditions. A brief review of the general frequency response characteristics of hydraulic shakers is also presented.

2.1 THRUST STAND

For this investigation a horizontal engine mount and thrust stand system is considered. The configuration is shown in Fig. 1a, and its diagrammatic equivalent is shown in Fig. 1b.

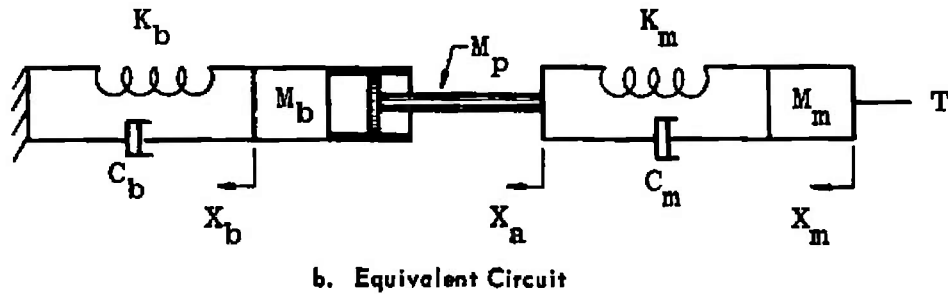
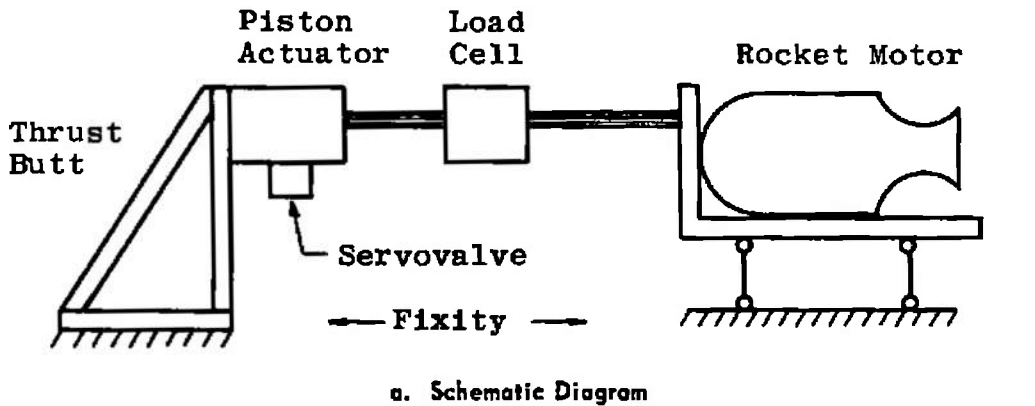


Fig. 1 Rocket Thrust Stand with Hydraulic Servo

The engine is represented by a single mass,  $M_m$ , and the load cell by a spring-damper combination,  $K_m$  and  $C_m$ . Although the thrust butt is usually a complex structure, its response can be closely approximated by a second-order system. For this reason the thrust butt is represented by the spring, mass and damper,  $K_b$ ,  $M_b$ , and  $C_b$ , respectively. The equivalent mass,  $M_b$ , will also be assumed to include the mass of the actuator housing and servovalve. The mass of the piston, however, will be considered separately in the analysis. The displacements,  $X_m$ ,  $X_b$ , and  $X_a$ , are measurements with respect to prefire locations of the motor, piston, and actuator housing. So that qualitative comparisons of data can be made, the thrust,  $T$ , will be a limited ramp function. The rise time and maximum level will be varied.

## 2.2 PERFORMANCE GOAL

The primary purpose of the hydraulic servomechanism is to produce the necessary expansion,  $X_b - X_a$ , in the thrust link to hold the rocket motor at its original prefire position ( $X_m = 0$ ). Also, of major importance is (1) the peak value of  $X_m$  during the firing transient, (2) time required for  $X_m$  to reach zero, and (3) the manner of returning to zero (damping).

On the basis of the above requirements the control signal to the servoamplifier consists of varying amounts of the following signals: (1) load-cell output signal for speeding up the recovery time, (2) integral of  $X_m$  to make  $X_m$  in steady-state identically equal to zero, and (3) velocity and acceleration for damping control. The coefficients for each of these signals are determined by optimization using the repetitive operation feature of the computer.

## 2.3 HYDRAULIC SERVOSYSTEM

Hydraulic shakers are specially designed servosystems for producing artificial vibration environments. They are ruggedly constructed and capable of producing large forces at relatively high frequencies. Because of these characteristics the specifications of a commercially available hydraulic shaker were used in this investigation in order to arrive at realistic values for the servosystem.

### 2.3.1 System Description

The hydraulic shaker system to be used in the analysis and simulation to follow consists of an amplifier, servovalve, hydraulic amplifier, piston actuator, and feedback transducers. A block diagram of the system is shown in Fig. 2.

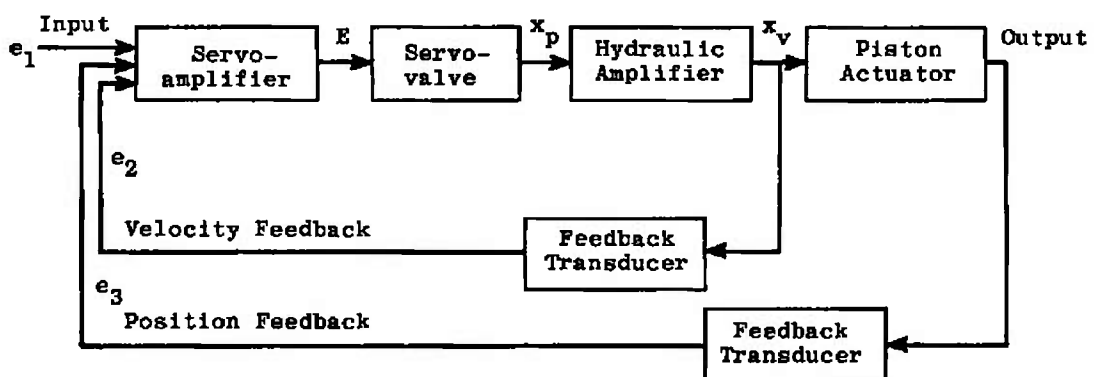


Fig. 2 Block Diagram of Hydraulic Shaker System

The servoamplifier is used to sum the input and feedback signals and to provide adjustable gain in the forward loop. The gains associated with the feedback signals are also adjustable. The amplifier produces a current in the coil of the electrohydraulic servovalve which, in turn, controls a flow to the hydraulic amplifier or power spool. The power spool then controls (with a large flow capability) the flow to the piston actuator.

In order to have fine prefire control in establishing a zero position for the rocket motor, the shaker system is connected as a positional servosystem. A signal proportional to the movement of the piston with respect to the actuator housing is fed back and compared to the input signal. Because the actuator is basically an integral device, a signal proportional to the flow to the actuator (position of the power spool) is fed back to add damping to the system.

### 2.3.2 Frequency Response Characteristics

The frequency response of a hydraulic shaker system is usually given in terms of relative output acceleration versus frequency. Relative acceleration,  $G$ , is the ratio of actual output acceleration to gravitational acceleration,  $g$ . Because the output acceleration is not only a function of the input signal, but also a function of load, the frequency response is represented by a family of curves. Each curve is the response for a single value of low resistance and massive load. A typical straight-line response is shown in Fig. 3 (Ref. 7).

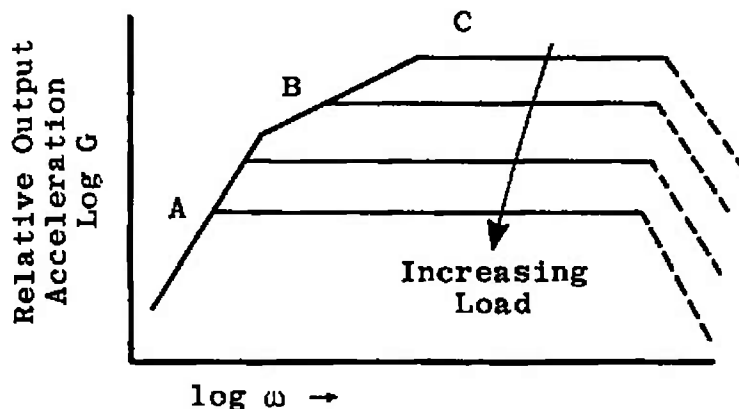


Fig. 3 Typical Hydraulic Shaker Frequency Response

Region A has a slope of 12 db per octave and is generally called the region of maximum stroke. Over this region the actuator excursions are limited only by the design limit of the actuator; reserve pressure is available for accelerating the load, and the servovalve is still capable

of supplying more flow if needed. Region B has a slope of 6 db per octave and is referred to as the valve flow limit region. In this region of operation, limiting velocity of the piston occurs as a result of the limiting flow through the servovalve. Region C is the region of constant acceleration. Here, not only limiting flow but an acceleration limit is present because all available pressure is being used to accelerate the load. Other break points, farther out in the frequency response, occur as a result of compressibility effects and servovalve response. For large loads, region B may not exist, and operation may only involve the stroke and acceleration limit regions.

For a fixed load condition and a constant-amplitude input signal, the shaker system can be represented by the following transfer function:

$$G(s) = \frac{K s^2}{(T_a s + 1)(T_b s + 1)(T_c s + 1)} \quad (1)$$

A straight-line logarithmic magnitude plot of this function is shown in Fig. 4.

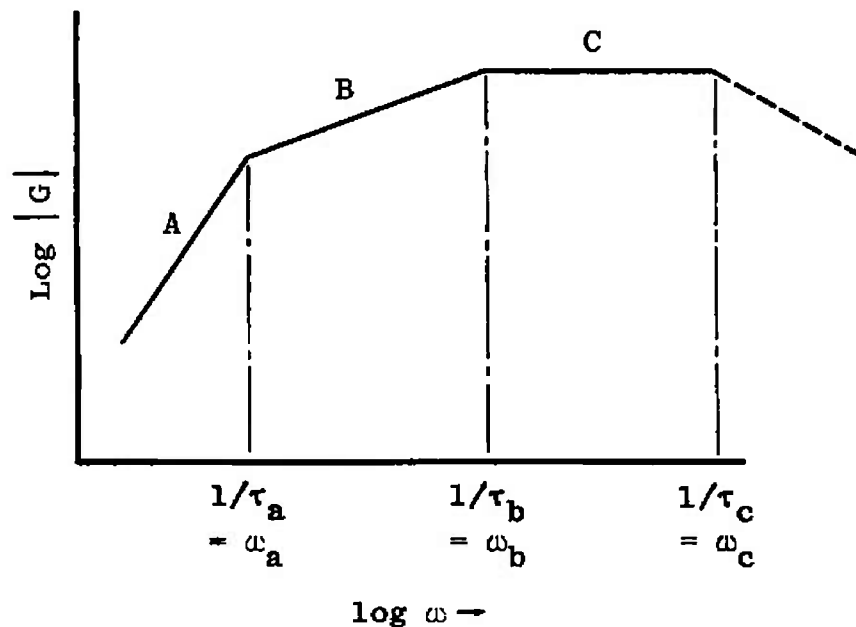


Fig. 4 Response for a Single Constant Load

The first break point,  $\omega_a$ , is fixed by the servovalve design. Investigation of typical commercial response curves indicates that  $\omega_a$  varies inversely with load, and  $\omega_c$  varies inversely with the load raised to some power in fitting the transfer function to the frequency response curves for other loads.

From the standpoint of analysis and simulation of the entire thrust stand system, Eq. (1) is of little value. The load on the hydraulic actuator varies drastically during the firing and tailoff transients. A linear analysis would have little meaning, and the problem must be approached through a detailed analysis of individual components.

### SECTION III SYSTEM ANALYSIS AND COMPONENT SELECTION

This section will be concerned with a detailed analysis of the thrust system to be simulated. Describing equations will be developed and specific values or ranges of values will be assigned to the coefficients. In the case of commercial components such as in the hydraulic servo-system, specific models will be selected and the manufacturers literature used as a guide in determining transfer functions.

#### 3.1 THRUST BUTT

With reference to Fig. 1, the thrust butt is to be represented by a linear second-order system. The force equation describing the dynamics of this system is

$$M_b s^2 X_b + C_b s X_b + K_b X_b = F_b \quad (2)$$

where  $F_b$  is the force transmitted by the hydraulic actuator. The mass,  $M_b$ , will be assumed to include the mass of the actuator housing, hydraulic amplifier, and servovalve.

The undamped natural frequency of this system is

$$f_n = \frac{1}{2\pi} \sqrt{\frac{K_b}{M_b}} \quad (3)$$

and the damping is

$$\zeta = \frac{1}{2} \frac{C_b}{\sqrt{K_b M_b}} \quad (4)$$

Under static load conditions the steady-state displacement is

$$X_{b_{ss}} = \frac{F_{b_{ss}}}{K_b} \quad (5)$$

Typical values of 40 cps undamped natural frequency, 0.008 damping ratio, and a displacement of 0.04 in. per 100,000 lbf leads to the following assigned values for the coefficients of Eq. (2):

$$\begin{aligned}K_b &= 2.5 \times 10^6 \text{ lb/in.} \\M_b &= 39.61 \text{ lb sec}^2/\text{in.} \\C_b &= 159.2 \text{ lb sec/in.}\end{aligned}$$

### 3.2 ENGINE AND LOAD-CELL COMBINATION

The mass of the rocket engine and the compliance and damping of the load cell form a mechanically tuned system. The force equation describing the dynamics of this system is

$$M_m s^2 X_m + C_m s (X_m - X_a) + K_m (X_m - X_a) = T_m \quad (6)$$

The force,  $T_m$ , is the thrust produced by the rocket motor. Depending on the size of the engine and the load cell, the damped natural frequency (for  $X_a = 0$ ) generally falls in the range from 30 to 50 cps. The frequency may vary during the firing of solid-propellant rocket engines because of the mass change caused by burning. So that the simulation will represent a worst case, the undamped natural frequency will purposely be set to 44 cps (slightly higher than the thrust butt frequency) and the damping to 0.008. The static displacement will be set for 0.1 in. per 100,000 lbf. The following assigned coefficients will produce a system with these characteristics:

$$\begin{aligned}K_m &= 1 \times 10^6 \text{ lb/in.} \\M_m &= 13.1 \text{ lb sec}^2/\text{in.} \\C_m &= 57.92 \text{ lb sec/in.}\end{aligned}$$

The force as seen by the load cell is

$$F_m = C_m s (X_m - X_a) + K_m (X_m - X_a) \quad (7)$$

so that Eq. (3) may be written as follows:

$$M_m s^2 X_m + F_m = T_m \quad (8)$$

### 3.3 HYDRAULIC ACTUATOR

The hydraulic actuator of Fig. 1 is shown in more detail in Fig. 5. For this analysis it will be assumed that the active areas of the piston are equal, and that the mass of the piston,  $M_p$ , includes that of the

piston rod. Also, the piston seals will be assumed to have no leakage. The friction will be of the viscous type with no stiction.

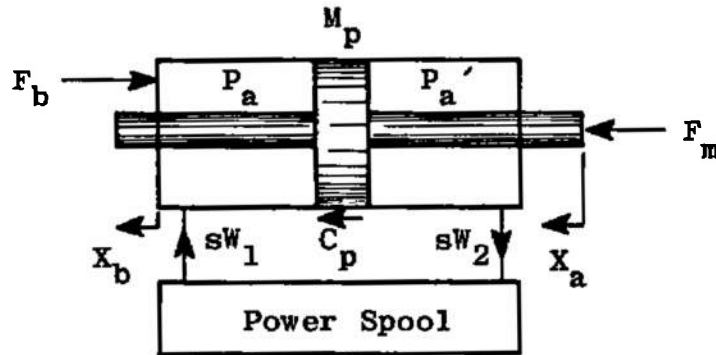


Fig. 5 Simplified Hydraulic Piston Actuator

### 3.3.1 Development of Describing Equations

The actuator force transmitted to the thrust butt is

$$F_b = P_a A_p - P_a' A_p - C_p s(X_b - X_a) \quad (9)$$

The force balance equation for the piston is

$$F_b = F_m - M_p s^2 X_a \quad (10)$$

The pressures on either side of the piston are functions of the position of the piston and of the fluids present. Stated mathematically the pressures are defined as follows:

$$P_a = \psi[(X_b - X_a), W_1] \quad (11)$$

$$P_a' = \delta[(X_b - X_a), W_2] \quad (12)$$

With time the dependent variable, the total derivative of  $P_a$  is

$$\frac{dP_a}{dt} = \left. \frac{\partial P_a}{\partial (X_b - X_a)} \right|_{W_1} \frac{d(X_b - X_a)}{dt} + \left. \frac{\partial P_a}{\partial W_1} \right|_{(X_b - X_a)} \frac{dW_1}{dt} \quad (13)$$

From the definition of bulk modulus,  $\beta$ , partial derivatives of Eq. (13) may be expressed as follows:

$$\frac{\partial P_a}{\partial (X_b - X_a)} = - \frac{\beta A_p}{V} \quad (14)$$

and

$$\frac{\partial P_a}{\partial W_1} = \frac{\beta}{\bar{w}V} \quad (15)$$

where  $V$  is the fluid volume in one end with the piston centered, and  $\bar{w}$  is the specific weight of the fluid. Substituting Eqs. (14) and (15) into Eq. (13) and taking the Laplace transform

$$sP_a = \frac{\beta}{\bar{w}V} sW_1 - \frac{\beta A_p}{V} s(X_b - X_a) \quad (16)$$

In like manner Eq. (12) may be written

$$sP'_a = -\frac{\beta}{\bar{w}V} sW_2 + \frac{\beta A_p}{V} s(X_b - X_a) \quad (17)$$

Equations (9), (10), (16), and (17) describe the dynamics of the actuator in terms of system variables. To arrive at an expression that will more qualitatively indicate response, the undamped natural frequency and damping of the actuator must be determined.

Integrating Eqs. (16) and (17) with respect to time, and multiplying each by the active area of the piston, yields

$$P_a A_p = \frac{\beta A_p W_1}{\bar{w}V} - \frac{\beta A_p^2}{V} (X_b - X_a) \quad (18)$$

$$P'_a A_p = -\frac{\beta A_p W_2}{\bar{w}V} + \frac{\beta A_p^2}{V} (X_b - X_a) \quad (19)$$

Substituting Eqs. (18) and (19) into Eq. (9)

$$\begin{aligned} \frac{\beta A_p W_1}{\bar{w}V} - \frac{\beta A_p^2}{V} (X_b - X_a) + \frac{\beta A_p W_2}{\bar{w}V} - \frac{\beta A_p^2}{V} (X_b - X_a) \\ = F_m - M_p s^2 X_a + C_p s (X_b - X_a) \end{aligned} \quad (20)$$

or

$$\begin{aligned} s^2 X_a + \frac{C_p}{M_p} s X_a + \frac{2\beta A_p^2}{VM_p} X_a = \frac{F_m}{M_p} + \frac{C_p}{M_p} s X_b \\ - \frac{\beta A_p W_1}{M_p \bar{w}V} + \frac{\beta A_p^2}{VM_p} X_b - \frac{\beta A_p W_2}{\bar{w}VM_p} + \frac{\beta A_p^2}{VM_p} X_b \end{aligned} \quad (21)$$

From Eq. (21) the undamped natural frequency of the actuator is

$$f_n = \frac{1}{2\pi} \sqrt{\frac{2\beta A_p^2}{VM_p}} \quad (22)$$

and the damping coefficient is calculated as follows:

$$\begin{aligned}
 2\zeta \omega_n &= \frac{C_p}{M_p} \\
 \zeta &= \frac{C_p}{2M_p} \sqrt{\frac{VM_p}{2\beta A_p^2}} \\
 &= \frac{C_p}{2A_p} \sqrt{\frac{V}{2\beta M_p}} \quad (23)
 \end{aligned}$$

for constant  $X_b$ ,  $W_1$ , and  $W_2$ . The frequencies observed with a simple actuator and massive load cannot be entirely predicted with Eq. (22) for the following reasons:

- (1) The analysis leading to Eq. (22) did not account for stiction, Coulomb friction, and leakage past the piston. Even if these nonlinearities did not exist, the damped natural frequency would be lower than the undamped natural frequency given by Eq. (13) as a function of damping.
- (2) Under some conditions of excitation, cavitation occurs, alternately making  $P_a$  and  $P_a'$  approximately zero. This effect tends to reduce the natural frequency by  $\frac{1}{\sqrt{2}}$ .
- (3) Oscillations about an off-center point where the two fluid volumes are not equal causes the fluid compliance to be greater in one direction than in the other. This causes the observed frequency to be higher and more distorted.

For simulation purposes the primary use of Eq. (23) is to determine the value of  $C_p$  for a desired value of damping. This will be needed when numerical values are assigned to the coefficients of the describing equations.

### 3.3.2 Actuator Specifications

For this simulation study an actuator with the following specifications was selected (Ref. 8):

Maximum dynamic force	100,000 lb
Maximum stroke	2 in. DA
Maximum velocity	9 in./sec
Piston weight	220 lb
Active piston area	41.67 in. <sup>2</sup>
Total fluid volume	102.0 in. <sup>3</sup>

The hydraulic fluid will be assumed to have a bulk modulus of 250,000 psi and a specific weight of 53 lb/ft<sup>3</sup>. Using Eq. (23), the value of  $C_p$  for a damping coefficient of 0.2 and other coefficients in agreement with the above specifications is as follows:

$$\begin{aligned} C_p &= 2A_p \zeta \sqrt{\frac{2\beta M_p}{V}} \\ &= 2(41.67)(0.2) \sqrt{\frac{2(0.25 \times 10^6)(220/386)}{102/2}} \\ &= 1245.0 \text{ lb sec/in.} \end{aligned}$$

### 3.4 SERVOVALVE AND HYDRAULIC AMPLIFIER

With reference to Fig. 2, the transfer function for the servovalve and hydraulic amplifier to be used in the simulation study are as follows (Ref. 9):

$$\frac{X_p}{E}(s) = \frac{K_1}{\left(\frac{s}{\omega_1} + 1\right) \left(\frac{s^2}{\omega_2^2} + \frac{2\zeta_2}{\omega_2} s + 1\right)} \quad (24)$$

$$\frac{X_v}{X_p}(s) = \frac{K_2}{s} \quad (25)$$

where

$$\omega_1 = 3768 \text{ radians/sec}$$

$$\omega_2 = 1884 \text{ radians/sec}$$

$$\zeta_2 = 0.25$$

The gains,  $K_1$  and  $K_2$ , as well as the gains of the servoamplifier and feedback transducers will not be specified since these will be adjusted for optimum performance prior to the collection of simulation data.

The flow specification for the selected valve is 100 gpm at 2500-psi pressure drop. Using the general flow equation for flow through a restriction,

$$Q = K' X_v \Big|_{\max} \sqrt{\Delta P} \quad (26)$$

or

$$K' X_v \Big|_{\max} = \frac{Q}{\sqrt{\Delta P}} = \frac{100}{\sqrt{2500}} = 2.0$$

and

$$K' = \frac{2}{X_v \Big|_{\max}} \quad (27)$$

In terms of weight flow, the flow equation can be written as follows:

$$sW = K' X_v (0.00223) \bar{w} \sqrt{\Delta P} \quad (28)$$

Substituting  $K'$  from Eq. (27),

$$sW = 0.00446 \bar{w} \frac{X_v}{X_v|_{\max}} \sqrt{\Delta P} \quad (29)$$

The quantity,  $\frac{X_v}{X_v|_{\max}}$ , is the normalized value of  $X_v$  and will be defined as follows:

$$\frac{X_v}{X_v|_{\max}} = X_{vn}, \quad (-1 \leq X_{vn} \leq +1)$$

With reference to Fig. 5, the flows  $\frac{dW_1}{dt}$  and  $\frac{dW_2}{dt}$  will be defined using Eq. (29) as follows:

$$sW_1 = 0.2364 X_{vn} \sqrt{P_s - P_a} \left. \vphantom{sW_1} \right\} \text{for } X_{vn} \text{ Positive} \quad (30)$$

$$sW_2 = 0.2364 X_{vn} \sqrt{P'_a - P_o} \left. \vphantom{sW_2} \right\} \quad (31)$$

and

$$sW_1 = 0.2364 X_{vn} \sqrt{P_a - P_o} \left. \vphantom{sW_1} \right\} \text{for } X_{vn} \text{ Negative} \quad (32)$$

$$sW_2 = 0.2364 X_{vn} \sqrt{P_s - P'_a} \left. \vphantom{sW_2} \right\} \quad (33)$$

The simulation circuit will be designed to select the appropriate flow equation by sensing the sign of  $X_{vn}$ .

#### SECTION IV SIMULATION RESULTS AND DISCUSSION

The equations resulting from the analysis of the thrust stand system were magnitude and time scaled (Appendix I). The scaled equations were then programmed on an analog computer to form an analog simulation of the system. Two computer circuits were used for the study: (1) simulation of the basic stand without the servosystem, and (2) simulation of the thrust stand system with the servo installed (Appendix II). Both simulation circuits were thoroughly checked for program and

wiring errors. They were then subjected to a series of operational checks to confirm static and dynamic performance.

This final section of this report will be concerned with an investigation of the performance of the thrust stand for different configurations. Both the time and frequency domains will be investigated and discussed in the material that follows.

#### 4.1 CONFIGURATION 1

In order to establish a reference for comparison purposes the basic thrust stand without the servo was investigated first. Figure 6 is a diagrammatic representation of this system.

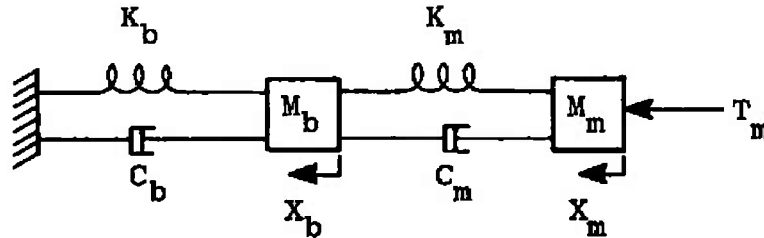


Fig. 6 Basic Thrust Stand without the Servo Installed

The equations describing the dynamics of this system are as follows:

$$M_b s^2 X_b + C_b s X_b + K_b X_b = F_m \quad (34)$$

$$M_m s^2 X_m + C_m s (X_m - X_b) + K_m (X_m - X_b) = T_m \quad (35)$$

$$F_m = C_m s (X_m - X_b) + K_m (X_m - X_b) \quad (36)$$

Using the same values for the constants in these equations as were used in the analysis, this system was subjected to several tests as explained below.

A limited ramp function was used for the thrust function. Several rise times varying from 0.2 to 0.01 sec were used with the limit level in every case set to 20,000 lb. The applied thrust functions,  $T_m$ , and the load-cell responses,  $F_m$ , were recorded as shown in Fig. 7. The ramp function was then replaced with a 1,000-lb peak sinusoidal thrust function. The frequency was varied to obtain the load-cell and motor position frequency responses shown in Fig. 8.

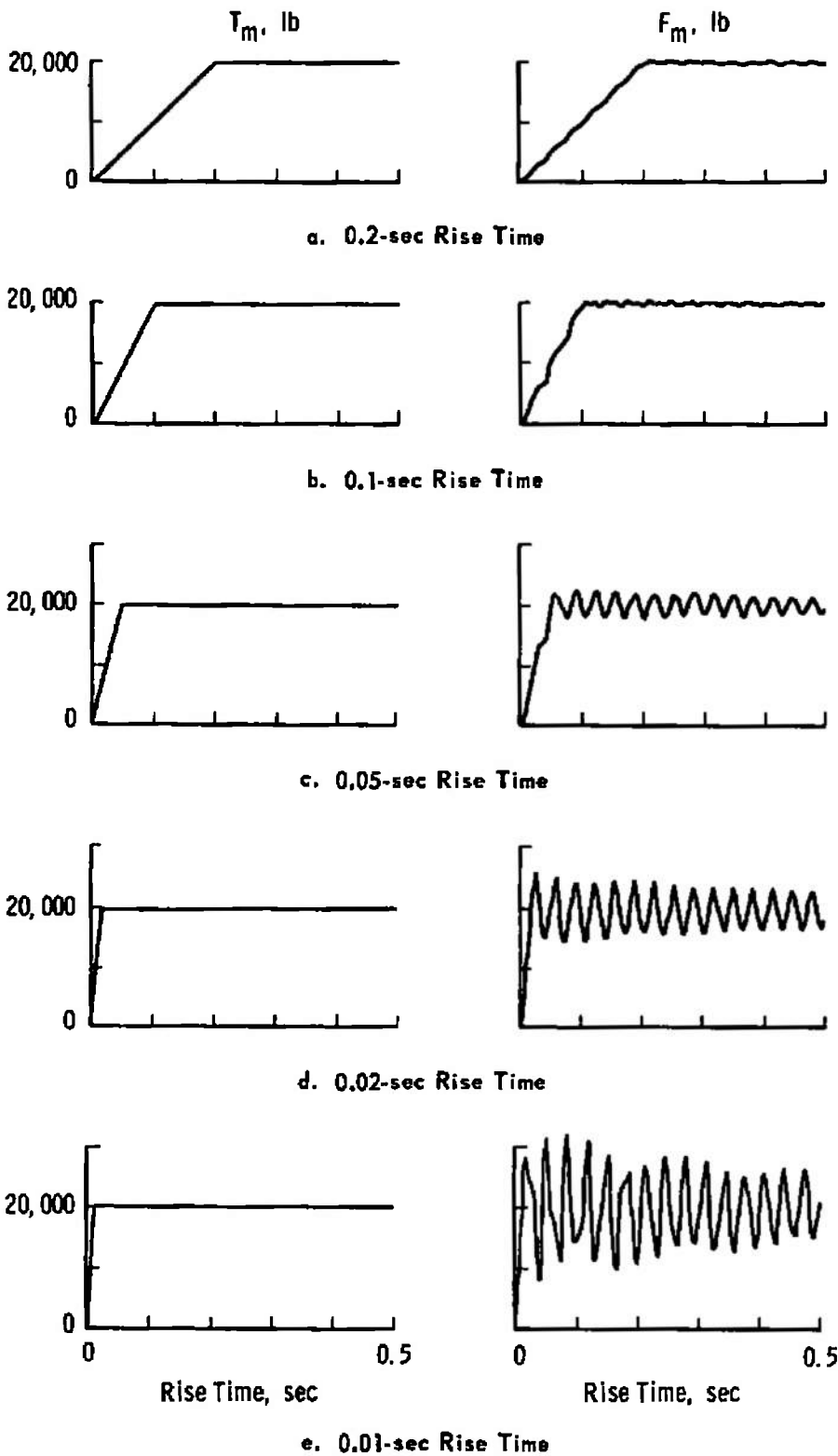


Fig. 7 Basic Thrust Stand Response to Varying Rise Times in Applied Thrust

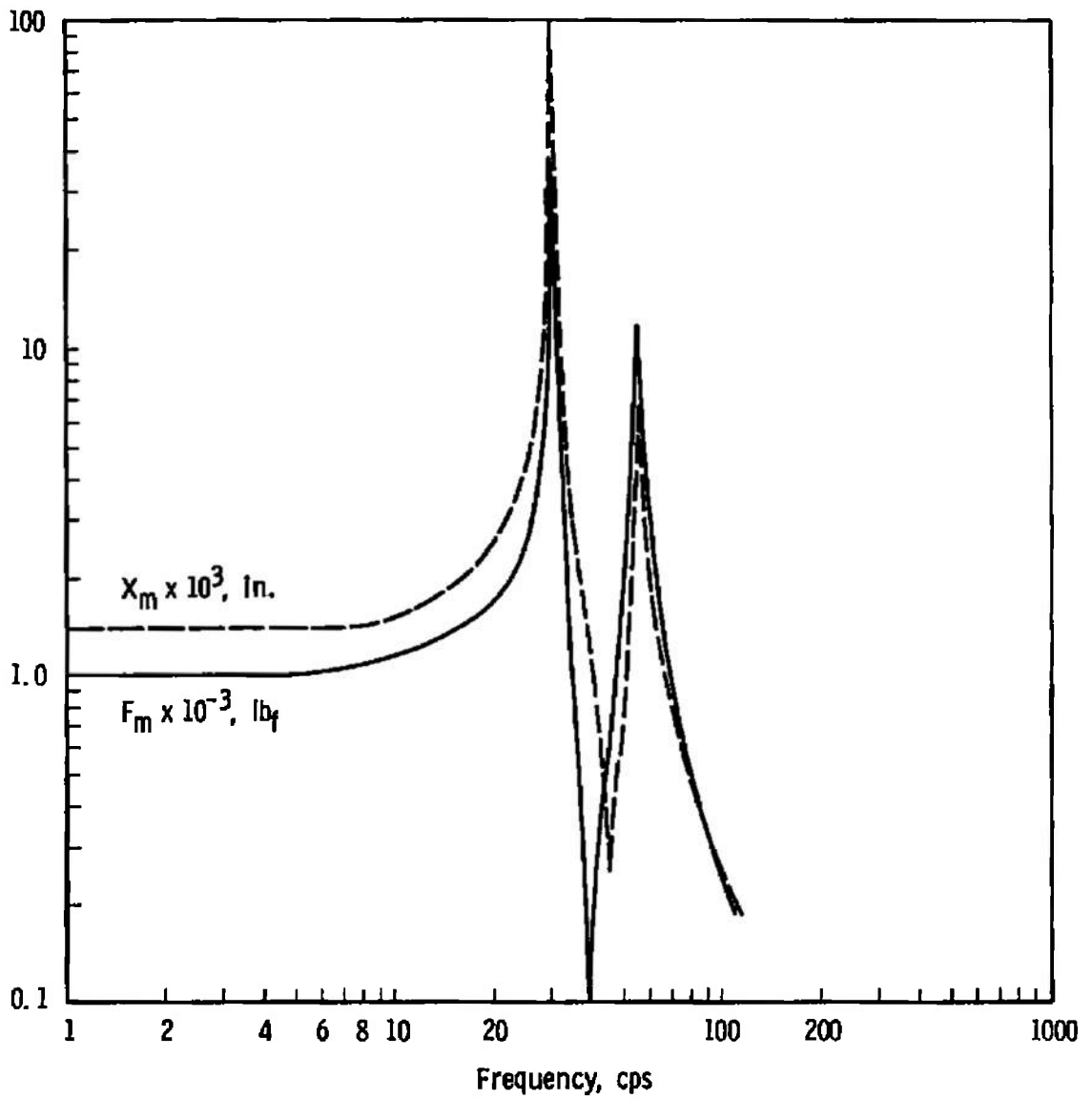


Fig. 8 Frequency Response of Basic Thrust Stand

In Fig. 8 the high Q resonance at 30 cps checks very closely with the damped natural frequency in Fig. 7 for the fastest rise times. The low frequency shift in the level of  $F_m$  in Fig. 7(e) occurring at approximately 5.5 cps is confirmed in Appendix III.

In order to check the resonant frequencies appearing in Fig. 8, Eqs. (34), (35), and (36) were solved simultaneously letting  $C_m = C_b = 0$  to yield the following auxiliary equation (set  $F_m = 0$  and substitute  $r$  for  $s$ )

$$r^4 + \frac{K_m K_b + K_b M_m + K_m M_m}{M_m M_b} r^2 + \frac{K_m K_b}{M_m M_b} = 0 \quad (37)$$

Since the complex roots of a polynomial with real coefficients occur in conjugate pairs and for this check the real parts are known to be zero ( $C_m = C_b = 0$ ), the roots of Eq. (37) provide only two frequencies. Substituting the assigned numerical values for the constants in Eq. (37) and factoring, the roots are found to be 31 and 56.7. These values check very closely to the resonant frequencies of 30 and 55 cps shown in Fig. 8. The resonant frequencies should be slightly below the undamped natural frequencies calculated above.

## 4.2 CONFIGURATION 2

The thrust stand system with the servo installed is considered in this investigation. The servo is connected as a positional servosystem where the command signal is furnished by the manual set-point potentiometer, and the piston position,  $X_b - X_a$ , is the feedback signal. Because the piston is basically an integral device (for light loads and negligible compression of the hydraulic fluid), the position of the power spool is proportional to the piston velocity. A proportional amount of the power spool position,  $X_v$ , is fed back to provide damping to the servosystem.

Starting with a very small damping signal, the servo gain was adjusted for a stable but slightly oscillatory response for a small step change in the manual set-point signal (10 percent). The responses of  $X_b - X_a$ ,  $X_v$ , and  $F_m$  were observed on the repetitive display scope of the computer. With each increase in the servo gain, the damping was increased, accordingly. A point was finally reached where a more stable operation could not be gotten by increasing the damping adjustment. At this point the servo gain was lowered slightly and the damping adjusted for optimum response. The data of Fig. 9 were then recorded.

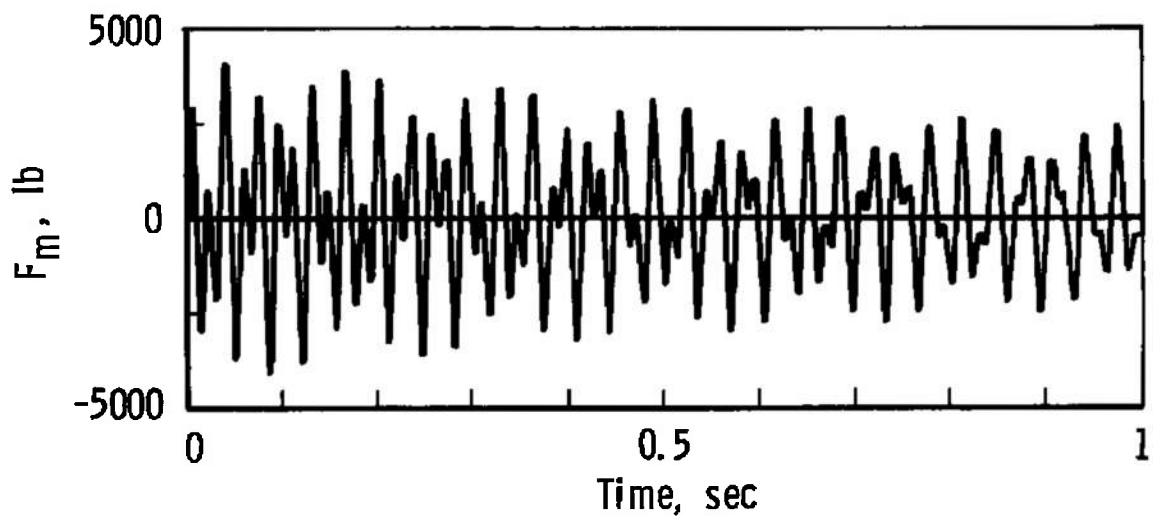
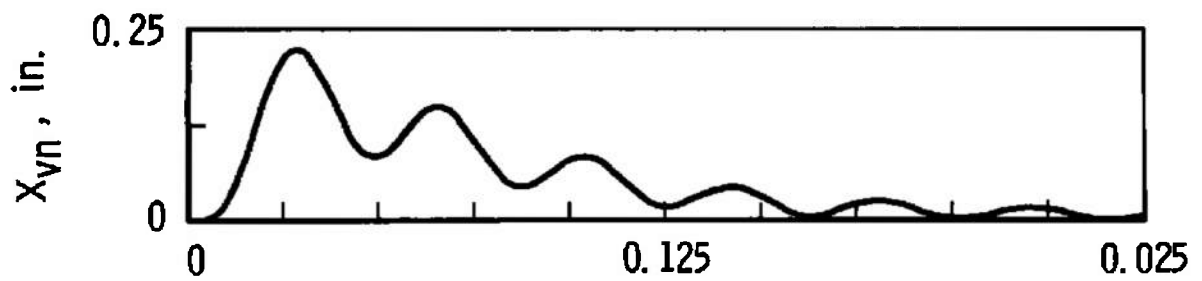
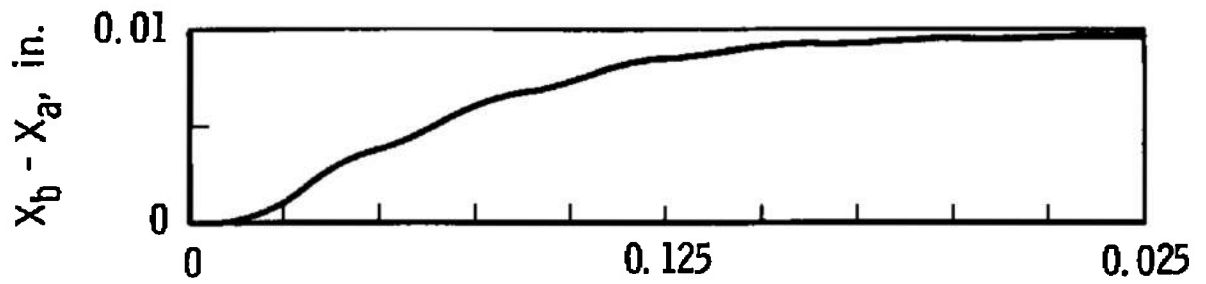


Fig. 9 Response in Manual Mode for Step Change in Servo Command Signal with Pilot Valve Damping Set for  $\zeta = 0.25$

The highly oscillatory response of  $X_v$  was investigated and found to be close to the damped natural frequency of the servovalve. The damping on the valve was increased from 0.25 to 0.7 and the data of Fig. 10 were recorded to show the effect. Comparing Figs. 9 and 10, the response of  $X_v$  was greatly affected, but that of  $X_b - X_a$  and  $F_m$  were affected only slightly. Because the damping was originally specified to be 0.25, and this would not normally be an adjustment on the servovalve, this value was used for the rest of the study.

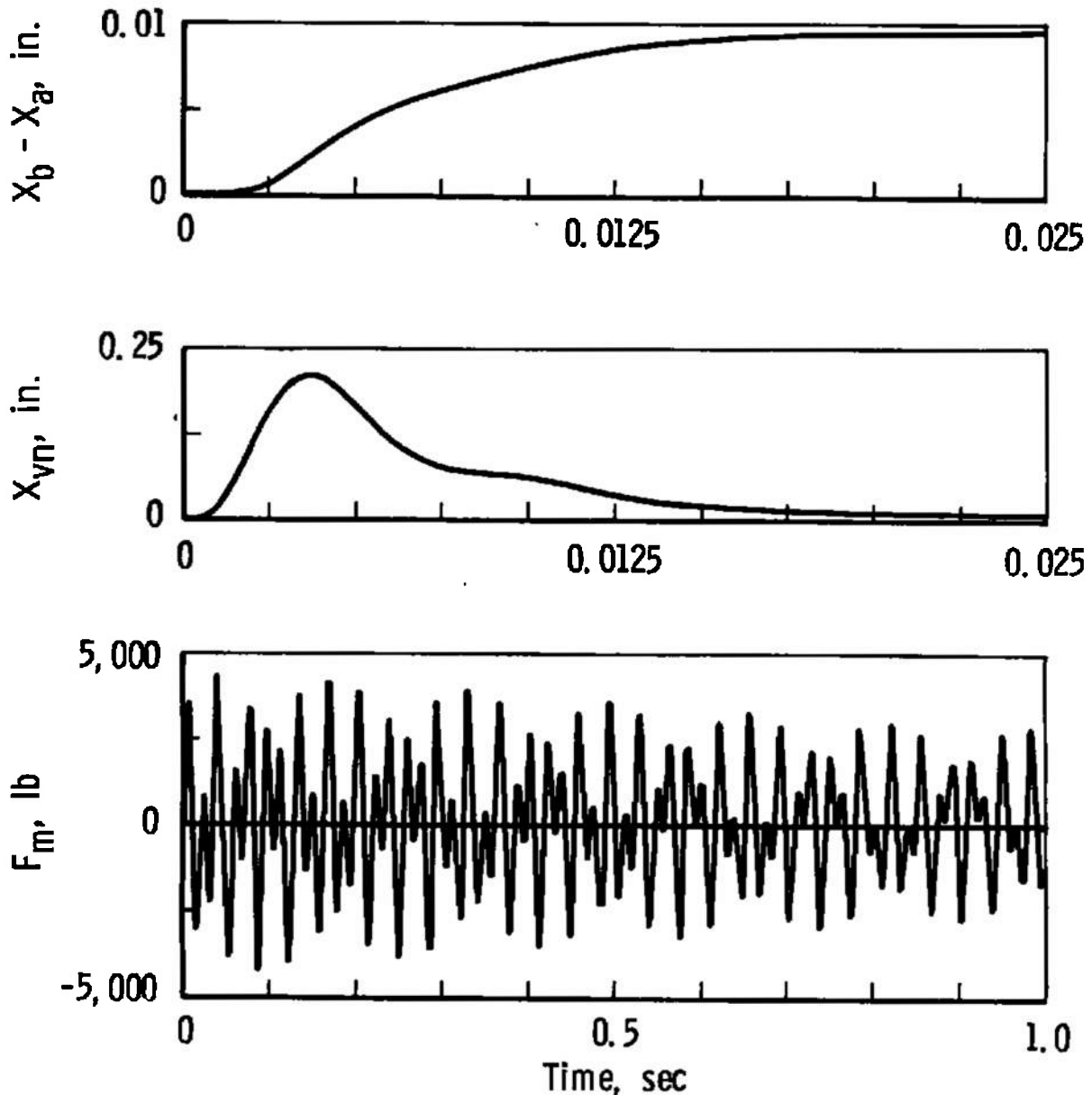


Fig. 10 Response in Manual Mode for Step Change in Servo Command Signal with Pilot Valve Damping Set for  $\zeta = 0.7$

In order to compare the performance of this configuration with that of Configuration 1, the system was tested with the same thrust functions (ramp and sinusoidal) to obtain the data shown in Figs. 11 and 12. Comparing Figs. 7 and 11, the load cell responses are almost identical, except that in Fig. 7 the damping is slightly less. The frequency responses of Figs. 8 and 12 are also very much alike except for the higher Q resonances in Fig. 8; this correlates well with the time responses since lower damping and higher Q are directly related.

### 4.3 CONFIGURATION 3

This investigation will be concerned with the automatic mode of operation. In this mode the command signal to the servo (replacing the manual set-point signal) is derived from live measurements from the rocket motor and thrust stand. For reasons explained below, the composite signals considered practical for this purpose are the load-cell output,  $F_m$ , and the rocket motor velocity and acceleration,  $sX_m$  and  $s^2X_m$ , respectively. The gain and damping determined in Configuration 2 for the servosystem is also used here since the servosystem is still used to position the piston actuator.

The composition of the automatic feedback signal was determined primarily on the basis of the practical aspects of the problem. Generally,  $F_m$ ,  $sX_m$ , and  $s^2X_m$  are readily available from single instruments with only minor instrumentation problems. Direct measurement of motor position is practically impossible in a test cell because of the absence of a fixed reference. Measurement of motor position by integration of the velocity is accompanied by noise and drift problems.

In order to satisfy the performance goal of zero motor position during the steady portion of the firing, a signal proportional to the steady level of thrust was needed. This was provided by the load cell output since  $T_m$  is equal to  $F_m$  in steady state. For zero rocket motor position in steady state, the position of the piston is related to the load-cell output by the following equation:

$$\begin{aligned} X_b - X_a &= \left( \frac{1}{K_m} + \frac{1}{K_b} \right) F_m \\ &= K_t F_m \end{aligned} \tag{38}$$

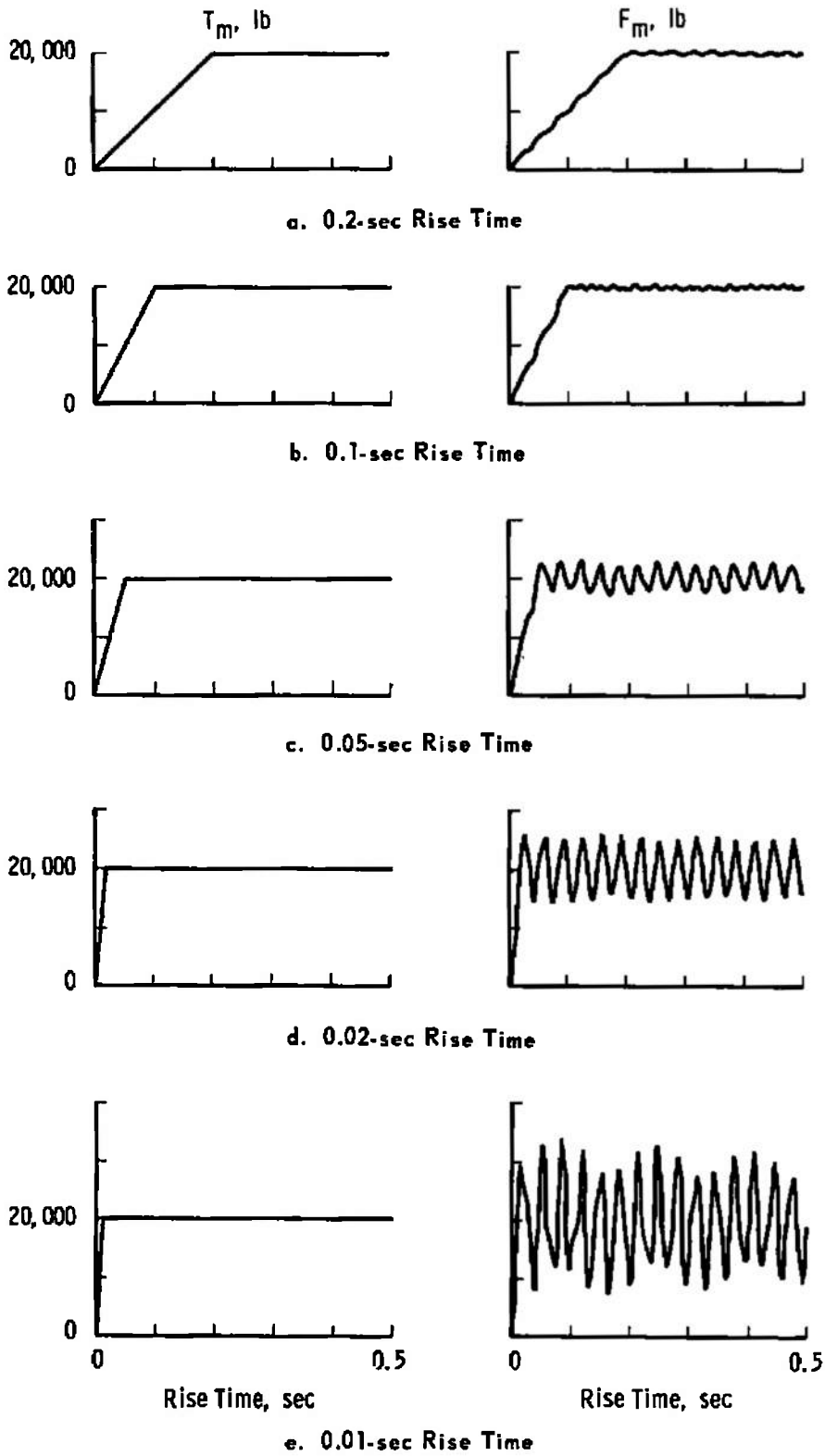


**Fig. 11 Response in Thrust Stand with Servo in Manual Mode for Varying Rise Times in Applied Thrust**

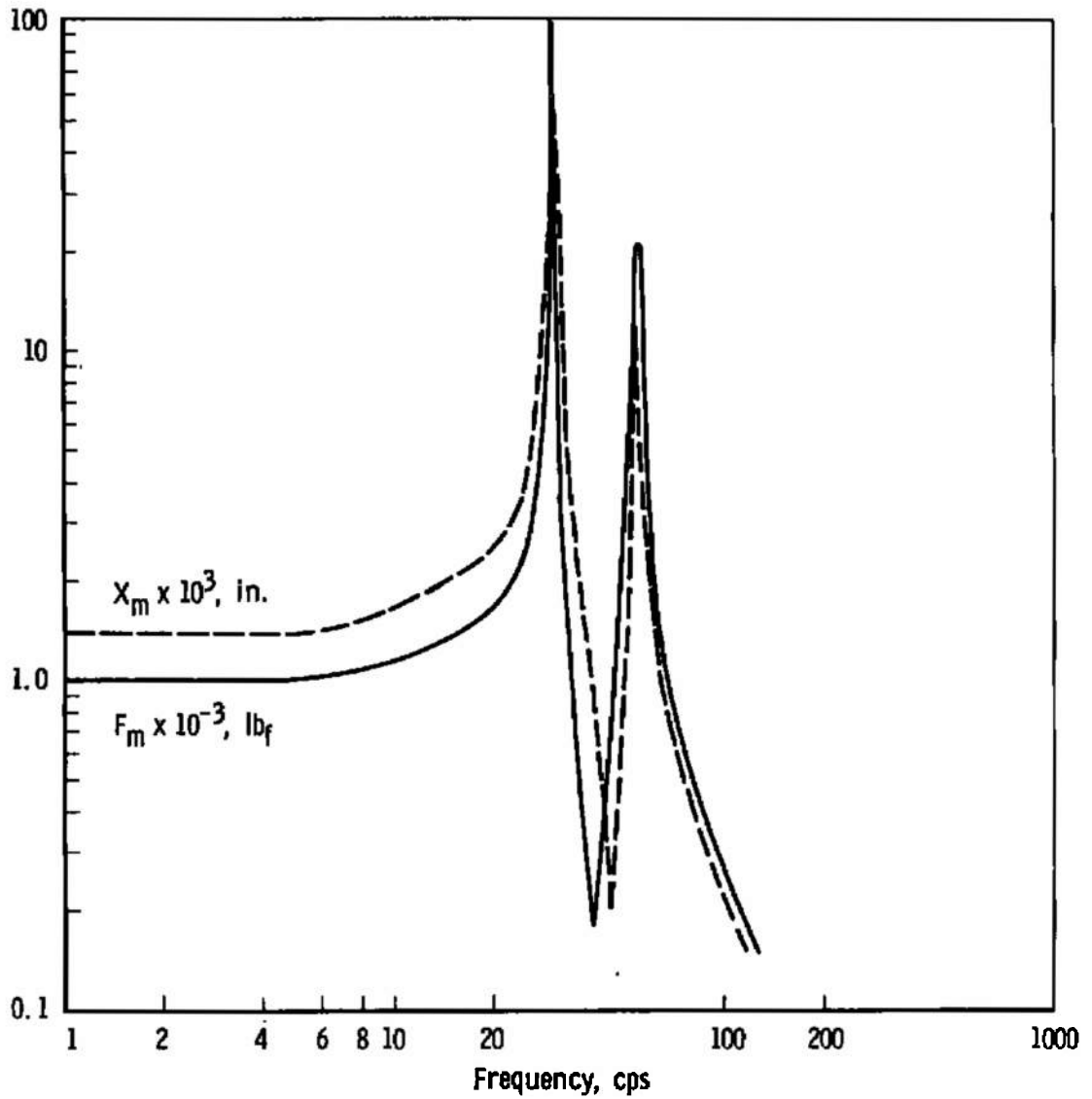
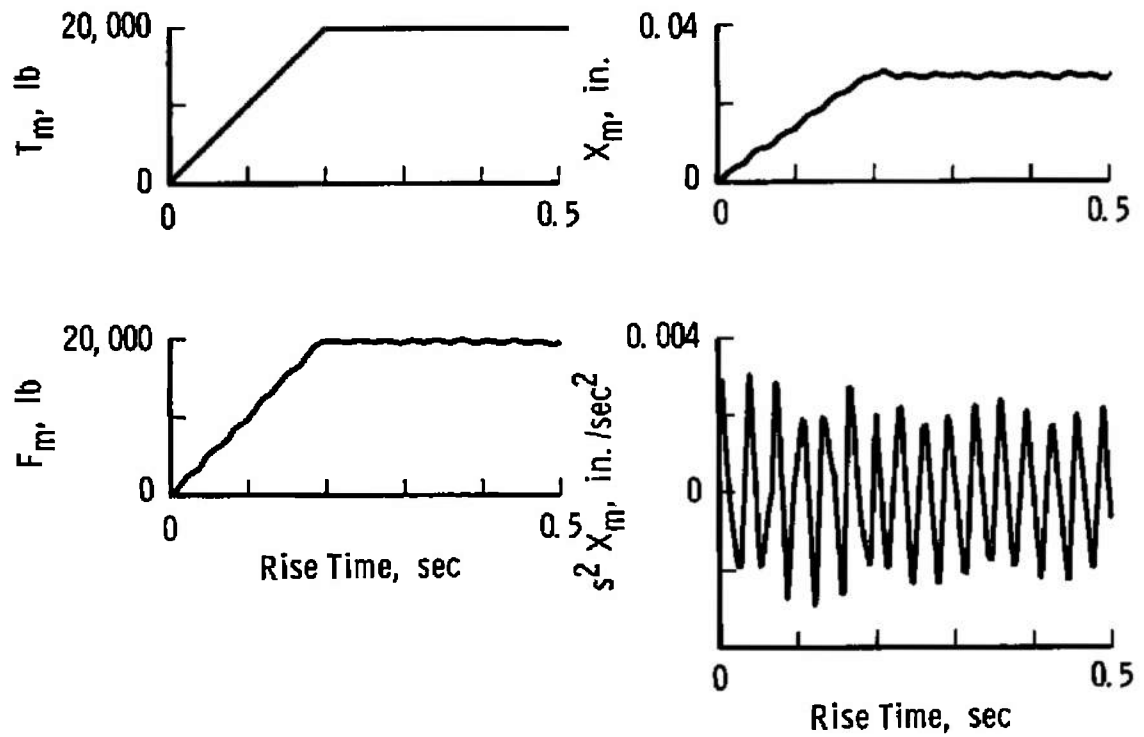


Fig. 12 Frequency Response of Thrust Stand System in the Manual Mode

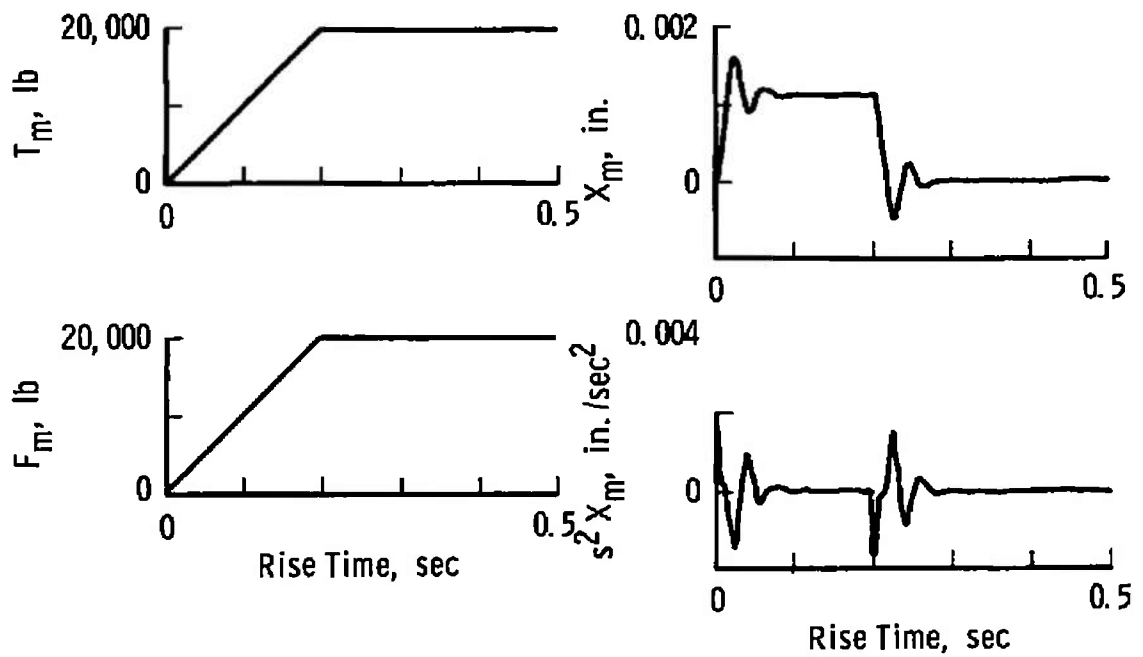
Feeding  $K_t F_m$  to the servoamplifier in the simulation caused the system to become unstable. This condition was brought under control by introducing a proportional amount of motor acceleration. Velocity was also added with some improvement. After optimizing the gains associated with velocity and acceleration in the feedback path, the gain on the velocity term was so small that this signal was removed before any data were recorded.

Figures 13 and 14 show the response of the thrust system. Figures 13a and 14a show the response for ramp thrust functions of 0.2- and 0.01-sec rise times in the manual mode with the manual set-point potentiometer set to zero. Figures 13b and 14b show the responses to the same thrust functions in the automatic mode with the active feedback set to  $K_t F_m$  plus an optimized amount of  $s^2 X_m$ . The limit level of the thrust function in every case was 20,000 lb. With the same feedback, the ramp thrust function was replaced with a sinusoidal thrust function (1000-lb peak) and the frequency response data of Fig. 15 were collected. The following characteristics and improvements may be seen from these data and comparisons to previously discussed data:

1. A high degree of damping has been introduced into the system in the automatic mode as seen by the time responses of Figs. 13 and 14. In the frequency domain this damping has greatly reduced the  $Q$  of the resonances. Notice, too, that the resonant frequencies have been slightly shifted.
2. In the low frequency region of both Figs. 8 and 12 the response of the motor position is flat, indicating that over this frequency range the position is directly proportional to the thrust amplitude. In Fig. 15 the closed loop control has provided a high degree of attenuation, especially in the low frequency region of  $X_m$ . The motor position is not only proportional to thrust amplitude but also proportional to frequency; the slope is approximately 20 db/decade. The displacement at zero frequency (steady-state) is zero as shown in Figs. 13b and 14b.
3. Comparing the frequency responses of the basic stand (Fig. 8) with those of Fig. 15, the automatic mode has extended the frequency response of the load cell and reduced that of the rocket motor position. Poor response in the rocket motor position at higher frequencies is favorable toward reducing the offset during the firing transient.

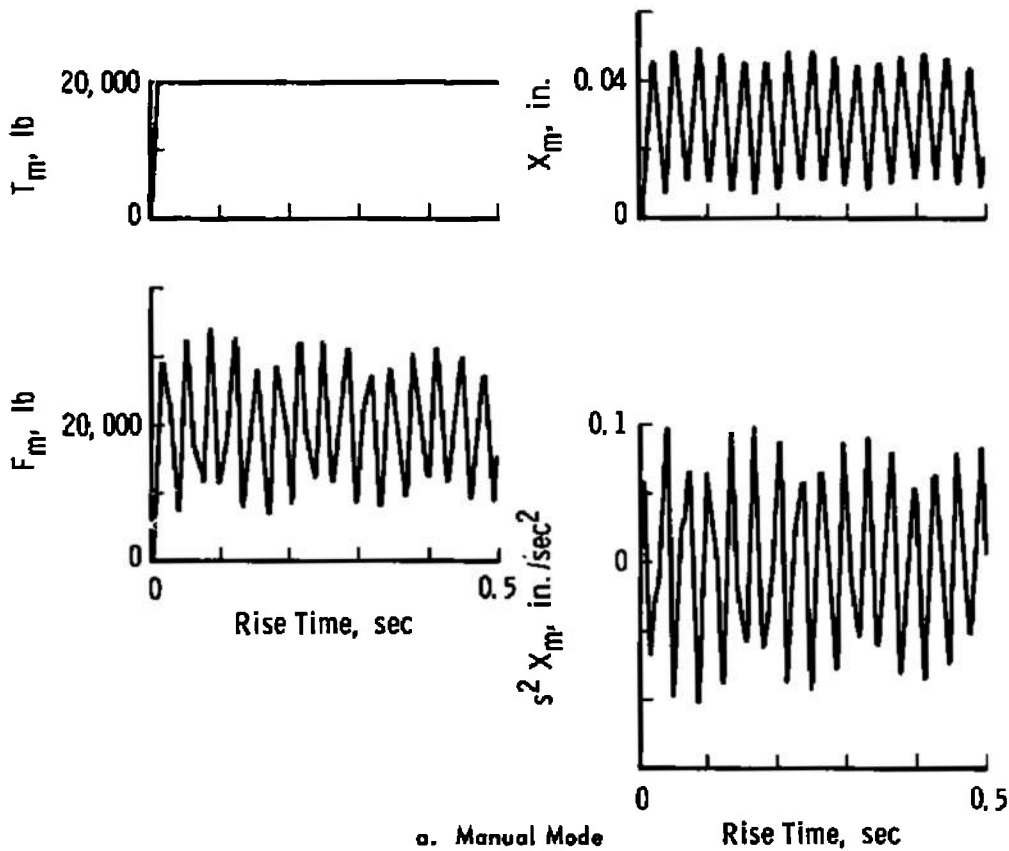


a. Manual Mode

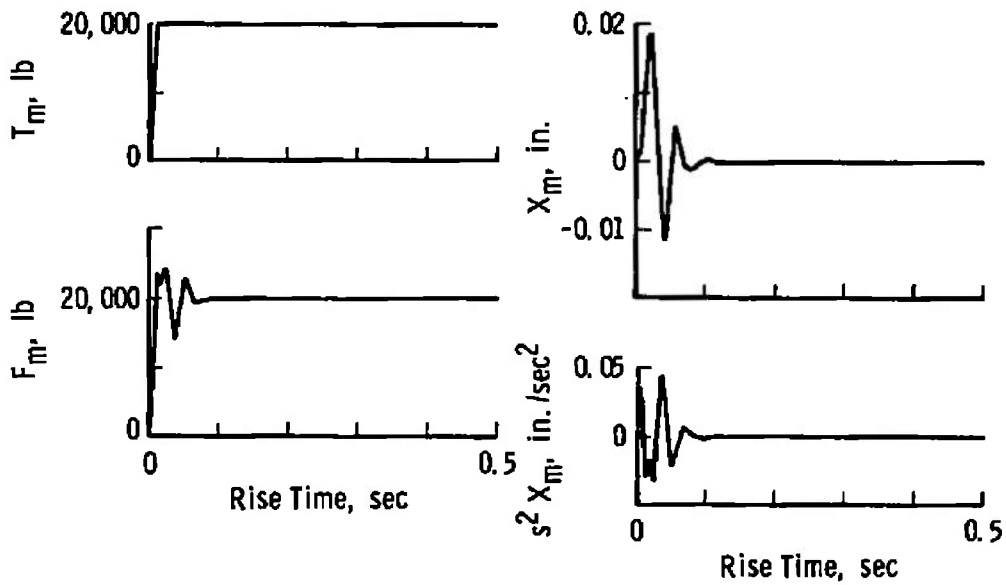


b. Automatic Mode

Fig. 13 Response of Thrust Stand for Varying Rise Time in Applied Thrust



a. Manual Mode



b. Automatic Mode

Fig. 14 Response of Thrust Stand for a 0.01-sec Rise Time Thrust Function

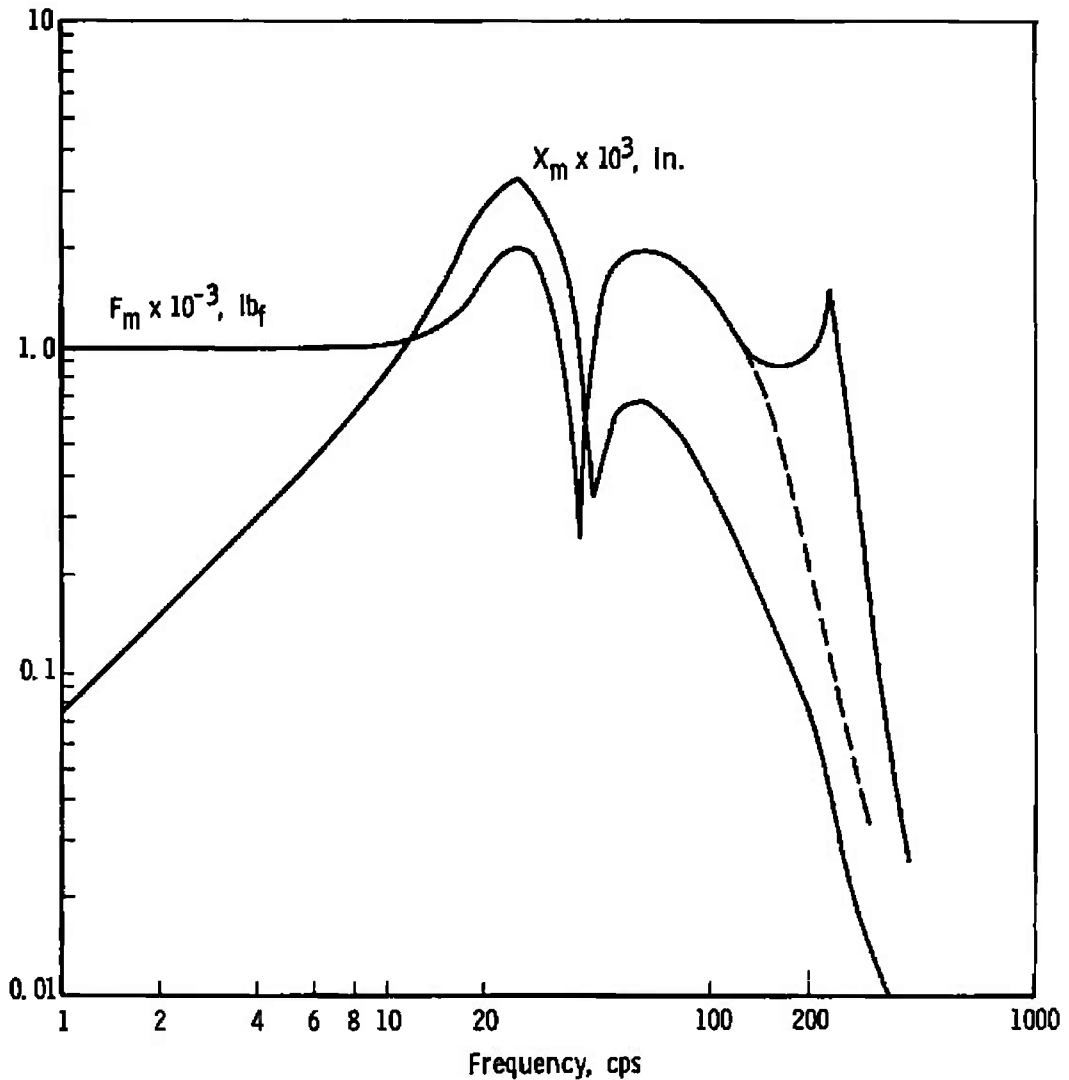


Fig. 15 Frequency Response of Thrust Stand System in the Automatic Mode

4. In Fig. 8, the resonance at 235 cps was investigated and found to be caused by the resonant frequency of the servomotor. This is slightly less than the damped natural frequency of 260 cps observed in the response of  $X_y$  in Fig. 9. The damping of the servomotor was increased from 0.25 to 0.5, and the frequency response of  $F_m$  checked again. The response below 100 cps remained unchanged but that in the high frequency range followed the dotted portion of the curve shown in Fig. 15.
5. For rocket motors where there is no steady portion of the firing but a steady drop in thrust, the position of the rocket motor will take on a value proportional to the slope of the

thrust (lb/sec). This is obvious from the time response of  $X_m$  in Fig. 13b during the rise time of the thrust function. This could be corrected by introducing a small amount of the integral of position as part of the feedback signal. Another way might be to use a signal which is composed of proportional plus derivative of the load-cell output. In any event, the correcting signal would be small (dependent on the slope of the thrust function) in most cases, which would favor the problem of working with integrators or adding lead networks.

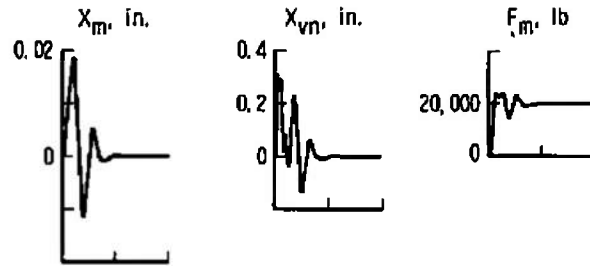
The ramp and sinusoidal thrust functions used thus far have been small enough to ensure operation within limiting velocity limits. As the thrust level goes up, however, the piston is required to move faster and over a greater amplitude, and limiting velocity begins to affect the response. Figure 16 shows the response of motor position and the load cell output for various levels of applied thrust. The rise time of the thrust functions is 0.01 sec in every case. Remembering that the normalized value of  $X_v$  is  $X_{vn}$ , which ranges in value from -1 to 1, the exact point at which limiting velocity occurs can be observed.

For thrust levels up to 60,000 lb the responses of  $X_m$  and  $F_m$  appear nearly linear. Limiting velocity is just reached when the thrust function is increased to 70,000 lb. Beyond this value the flow limit is reached more than once, and the response of  $F_m$  becomes noticeably affected. For the 80,000-lb thrust function the pressure  $P'_a$  dropped to 9.5 psia. Then, for 90,000 lb thrust,  $P'_a$  dropped to 4 psia. This is the region at which cavitation occurs and the equations concerning flow become invalid.

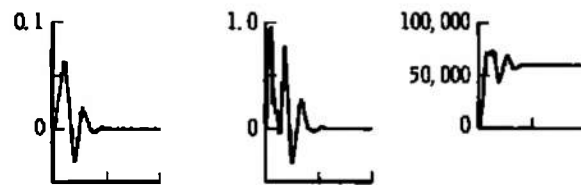
## SECTION V CONCLUSIONS

The results of this simulation study indicate that the dynamic response of existing thrust stands can be greatly improved using a high quality servosystem. A system similar to Configuration 3 would provide the following improvements in comparison to a basic stand.

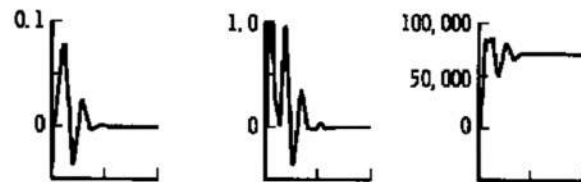
1. A high degree of system damping would be introduced.
2. Immediately after the firing transient the rocket motor would return to its initial prefire position. The motor would remain at this position even for moderately rapid changes in thrust level because of the fast tracking capability of the servosystem.



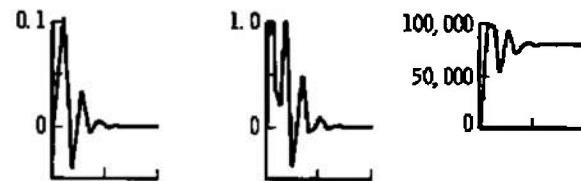
a. 20,000-lb Applied Thrust



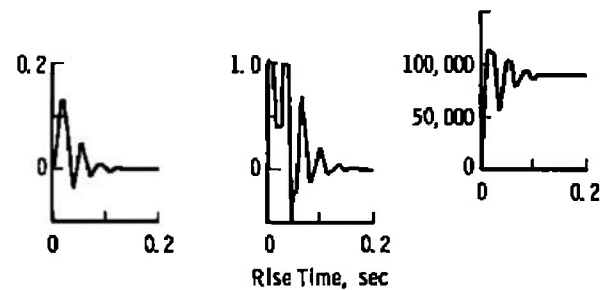
b. 60,000-lb Applied Thrust



c. 70,000-lb Applied Thrust



d. 80,000-lb Applied Thrust



e. 90,000-lb Applied Thrust

**Fig. 16 Response of Thrust Stand in the Automatic Mode to Varying Thrust Levels with 0.01-sec Rise Times**

3. Optimization of the control circuitry would greatly decrease the offset of the motor position during the firing transient.
4. Concurrent with the improvements described above, the acceleration of the rocket would be greatly decreased during the firing and tailoff transients.

#### REFERENCES

1. McGregor, W. K. "Determination of Forcing Functions from the Response of a Known Physical System." Simulation Council Newsletter, Instruments and Control Systems, July 1959.
2. Sprouse, J. A. and McGregor, W. K. "Investigations of Thrust Compensation Methods." AEDC-TDR-63-85 (AD411841), August 1963.
3. Mason, M. S. and Clary, G. W. "A Computational Compensation for Measuring System Dynamics." Simulation, Vol. 7, No. 6, December 1966, p. 318.
4. Ormand, A. N. "Six-Component Rocket Motor Thrust Stand, Mod. MCT-1421-4K." Ormand, Inc. Technical Discussion No. 1421-1, Santa Fe Springs, Calif.
5. Inca Engineering Corporation. "Research Studies and Modification of Thrust Measuring System, Final Report." December 15, 1963.
6. Crosswy, F. L. "Investigation of Dynamic Thrust Measurement Techniques." Masters thesis, The University of Tennessee, Knoxville, Tennessee, June 1967.
7. Harris, C. M. and Crede, C. E. Shock and Vibration Handbook, Vol. 2, McGraw-Hill Book Company, New York, 1961.
8. Sipfle, R. "Approximate Oil Volumes for MB Hydraulic Shakers." Report IS-67-2, MB Electronics Company, New Haven, Conn.
9. Moore, W. C. "Frequency Response of HV80 and HV220 Servo Valves." Report IS-65-7, MB Electronics Company, New Haven, Conn.
10. Myklestad, N. O. Fundamentals of Vibration Analysis. McGraw-Hill Book Company, New York, 1956.

**APPENDIXES**

- I. TIME AND AMPLITUDE SCALING OF SYSTEM EQUATIONS**
- II. SIMULATION CIRCUITS**
- III. LOW FREQUENCY SHIFT IN THE RESPONSE OF  $F_m$**

**APPENDIX I**  
**TIME AND AMPLITUDE SCALING OF SYSTEM EQUATIONS**

The equations resulting from the analysis of the thrust system are summarized below. Some of the equations from the text have been arranged below so that they express the quantity to be solved for by the computer.

$$s^2 X_b = \frac{F_b}{M_b} - \frac{C_b}{M_b} s X_b - \frac{K_b}{M_b} X_b \quad (2)$$

$$F_m = C_m s(X_m - X_a) + K_m (X_m - X_a) \quad (7)$$

$$s^2 X_m = \frac{1}{M_m} (T_m - F_m) \quad (8)$$

$$F_b = (P_a - P_a') A_p - C_p s (X_b - X_a) \quad (9)$$

$$s^2 X_a = \frac{1}{M_p} (F_m - F_b) \quad (10)$$

$$s P_a = \frac{\beta}{wV} s W_1 - \frac{\beta A_p}{V} s (X_b - X_a) \quad (16)$$

$$s P_a' = - \frac{\beta}{wV} s W_2 + \frac{\beta A_p}{V} s (X_b - X_a) \quad (17)$$

$$X_p \left( \frac{s}{\omega_1} + 1 \right) = \frac{KE}{s^2 - 2 \zeta_2 \omega_2 s + \omega_2^2} \quad (24)$$

$$X_v = \frac{K}{s} X_p \quad (25)$$

$$s W_1 = 0.00446 \bar{w} X_{vn} \sqrt{P_s - P_a} \quad (30)$$

$$s W_2 = 0.00446 \bar{w} X_{vn} \sqrt{P_a' - P_o} \quad (31)$$

$$s W_1 = 0.00446 \bar{w} X_{vn} \sqrt{P_a - P_o} \quad (32)$$

$$s W_2 = 0.00446 \bar{w} X_{vn} \sqrt{P_s - P_a'} \quad (33)$$

The coefficients which apply to the above equations are summarized below:

$K_b = 2.5 \times 10^6 \text{ lb/in.}$	$\omega_1 = 3768.0 \text{ radians/sec}$
$M_b = 39.61 \text{ lb sec}^2/\text{in.}$	$\omega_2 = 1884.0 \text{ radians/sec}$
$C_b = 159.2 \text{ lb sec/in.}$	$\zeta_2 = 0.25$
$K_m = 1 \times 10^6 \text{ lb/in.}$	$\beta = 0.25 \times 10^6 \text{ psi}$
$M_m = 13.1 \text{ lb sec}^2/\text{in.}$	$M_p = 0.5699 \text{ lb sec}^2/\text{in.}$
$C_m = 57.92 \text{ lb sec/in.}$	$C_p = 1245.0 \text{ lb sec/in.}$
$A_p = 41.67 \text{ in.}^2$	$\bar{w} = 53.0 \text{ lb/ft}^3$
$V = 51.0 \text{ in.}^3$	

Substituting the above coefficients into the system equations and scaling the system variables so that the quantities,  $\left[ \frac{F}{10^3} \right]$ ,  $\left[ \frac{T}{10^3} \right]$ ,  $\left[ \frac{P}{30} \right]$ ,  $\left[ 100 W \right]$ , and  $\left[ 100 X_{VN} \right]$  appear, the equations become

$$s^2 \left[ 10^3 X_b \right] = 0.0524 \times 10^6 \left[ \frac{F_b}{10^3} \right] - 4.02 s \left[ 10^3 X_b \right] - 0.06311 \times 10^6 \left[ 10^3 X_b \right] \quad (2)$$

$$\left[ \frac{F_m}{10^3} \right] = 57.92 \times 10^6 s \left[ 10^3 X_m - 10^3 X_a \right] - 1.0 \left[ 10^3 X_m - 10^3 X_a \right] \quad (7)$$

$$s^2 \left[ 10^3 X_m \right] = 0.07633 \times 10^6 \left[ \frac{T_m}{10^3} - \frac{F_m}{10^3} \right] \quad (8)$$

$$\left[ \frac{F_b}{10^3} \right] = 1.25 \left[ \frac{P_a - P_a'}{30} \right] - 0.001245 s \left[ 10^3 X_b - 10^3 X_a \right] \quad (9)$$

$$s^2 \left[ 10^3 X_a \right] = 1.755 \times 10^6 \left[ \frac{F_m - F_b}{10^3} \right] \quad (10)$$

$$s \left[ \frac{P_a}{30} \right] = 53.27 s \left[ 100 W_1 \right] - 6.810 s \left[ 10^3 X_b - 10^3 X_a \right] \quad (16)$$

$$s \left[ \frac{P_a'}{30} \right] = -53.27 s \left[ 100 W_2 \right] - 6.810 s \left[ 10^3 X_b - 10^3 X_a \right] \quad (17)$$

$$X_p(2.654 \times 10^{-4} s + 1) = \frac{KE}{s^2 + 942s + 3.549 \times 10^6} \quad (24)$$

$$\left[ 100 X_{vn} \right] = \frac{K}{b} X_p \quad (25)$$

$$s \left[ 100 W_1 \right] = 1.295 \left[ 100 X_{vn} \right] \sqrt{\frac{P_s - P_a}{30}} \quad (30)$$

$$s \left[ 100 W_2 \right] = 1.295 \left[ 100 X_{vn} \right] \sqrt{\frac{P'_a - P_o}{30}} \quad (31)$$

$$s \left[ 100 W_1 \right] = 1.295 \left[ 100 X_{vn} \right] \sqrt{\frac{P_a - P_o}{30}} \quad (32)$$

$$s \left[ 100 W_2 \right] = 1.295 \left[ 100 X_{vn} \right] \sqrt{\frac{P_s - P'_a}{30}} \quad (33)$$

In order to facilitate the recording of simulation data on an X-Y recorder, the above scaled system equations are slowed down in time by a factor of 100. This is accomplished by letting  $s$  in the above equations be  $100s$ . In the time domain this is equivalent to letting

$$\frac{d}{dt} = 100 \frac{d}{d\tau}, \text{ where } \tau = 100t$$

The thrust function  $T_m$  which is a limited ramp function with rise times ranging from 0.01 to 0.2 sec will be time scaled accordingly so that the rise times from 1.0 to 20 sec will be used.

The final amplitude and time scaled system equations are as follows:

$$s^2 \left[ 10^3 X_b \right] = 2.524 \left[ \frac{F_b}{10^2} \right] - 0.0402s \left[ 10^3 X_b \right] - 6.311 \left[ 10^3 X_b \right] \quad (2)$$

$$\left[ \frac{F_m}{10^2} \right] = 0.005792 s \left[ 10^3 X_m - 10^3 X_a \right] + 1.0 \left[ 10^3 X_m - 10^3 X_a \right] \quad (7)$$

$$s^2 \left[ 10^3 X_m \right] = 7.633 \left[ \frac{T_m - F_m}{10^3} \right] \quad (8)$$

$$\left[ \frac{F_b}{10^3} \right] = 1.25 \left[ \frac{P_s - P'_a}{30} \right] - 0.1245 s \left[ 10^3 X_b - 10^3 X_a \right] \quad (9)$$

$$s^2 \left[ 10^3 X_a \right] = 175.5 \left[ \frac{F_m - F_b}{10^3} \right] \quad (10)$$

$$s \left[ \frac{P_a}{30} \right] = 53.27 s \left[ 100 W_1 \right] - 6.810 s \left[ 10^3 X_b - 10^3 X_a \right] \quad (16)$$

$$s \left[ \frac{P'_a}{30} \right] = -53.27 s \left[ 100 W_2 \right] + 6.810 s \left[ 10^3 X_b - 10^3 X_a \right] \quad (17)$$

$$X_p(0.02654 s + 1) = \frac{KE}{s^2 + 9.425 s + 354.9} \quad (24)$$

$$\left[ 100 X_{vn} \right] = \frac{K}{s} X_p \quad (25)$$

$$s \left[ 100 W_1 \right] = 0.01295 \left[ 100 X_{vn} \right] \sqrt{\frac{P_a - P_a}{30}} \quad (30)$$

$$s \left[ 100 W_2 \right] = 0.01295 \left[ 100 X_{vn} \right] \sqrt{\frac{P'_a - P_o}{30}} \quad (31)$$

$$s \left[ 100 W_1 \right] = 0.01295 \left[ 100 X_{vn} \right] \sqrt{\frac{P_a - P_o}{30}} \quad (32)$$

$$s \left[ 100 W_2 \right] = 0.01295 \left[ 100 X_{vn} \right] \sqrt{\frac{P_s - P'_a}{30}} \quad (33)$$

**APPENDIX II  
SIMULATION CIRCUITS**

The simulation circuit used for studying Configuration 1 is shown in Fig. II-1. Equations (2), (7), and (8) were used for this study by letting  $X_a = X_b$  and  $F_b = F_m$ . The scaled versions of these equations are shown at the end of Appendix I.

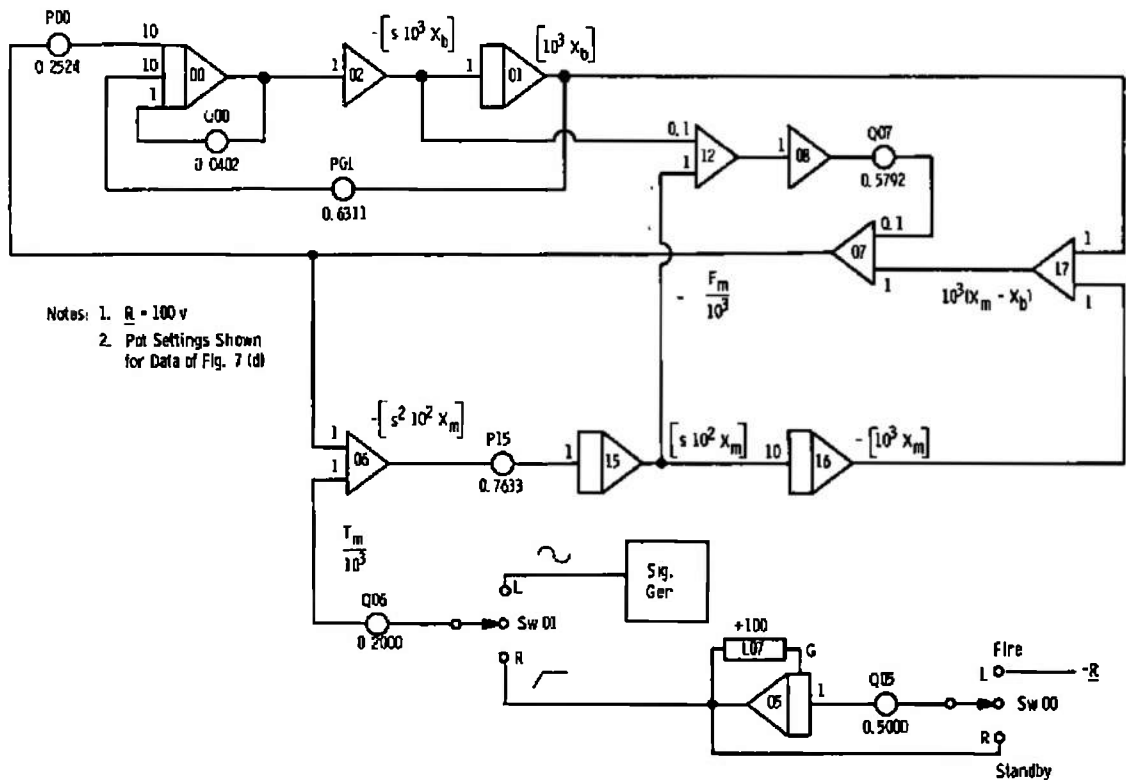


**Fig. II-1 Simulation of Basic Thrust Stand**

Figure II-2 is the analog circuit used for studying the second two configurations. This circuit is the analog program for Eqs. (2) through (33) at the end of Appendix I.

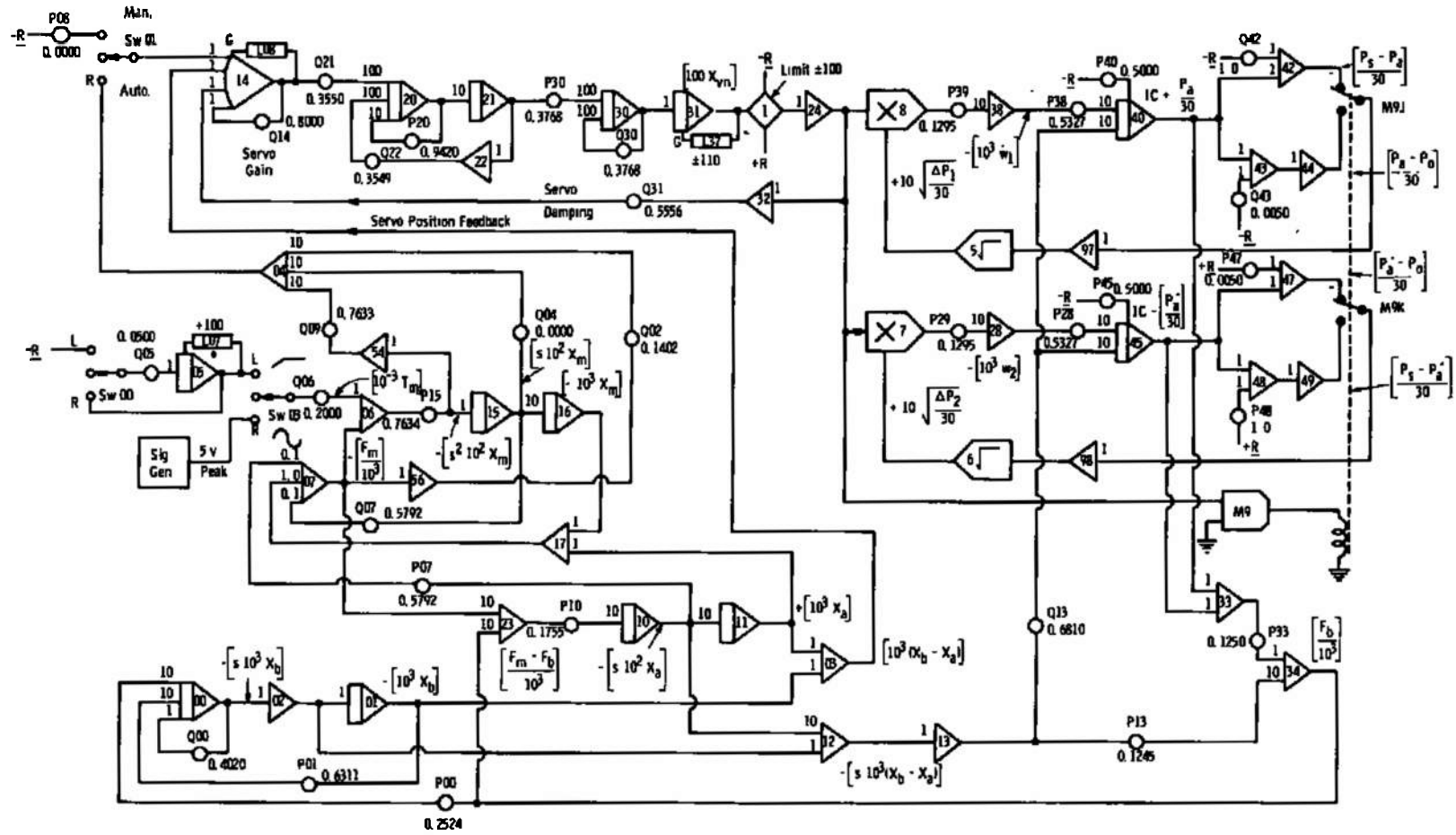


Fig. II-2 Simulation Circuit of Thrust Stand and Hydraulic Servosystem

**APPENDIX III  
LOW FREQUENCY SHIFT IN THE RESPONSE OF  $F_m$**

In Fig. 7e two frequencies are noticeable in the response of  $F_m$ ; these frequencies are approximately 30 and 5.5 cps. The 30-cps frequency is the damped natural frequency corresponding to the calculated undamped natural frequency of 31 cps. The 5.5-cps frequency is not easily related to either the 31- or 56.7-cps undamped natural frequencies or to combinations of the two. Since this low frequency is also present in the response of the rocket motor position (Fig. 14e), its presence in the response of  $F_m$  can best be explained by directing our attention to the analytic solution for  $X_m$  for the undamped system.

Letting  $C_b = C_m = 0$  in Eqs. (34), (35), and (36), and solving these equations simultaneously for  $X_m$ , an equation results having a general solution of the form (Ref. 10)

$$X_m = A_1 + A_2 - A_1 \cos \omega_1 t - A_2 \cos \omega_2 t \quad (\text{III-1})$$

At  $t = 0$ ,  $X_m = 0$  and at periodic time intervals later the cosine terms alternately add and subtract to produce variation in amplitude at the rate of 5.5 cps. This is confirmed in the computer investigation that follows.

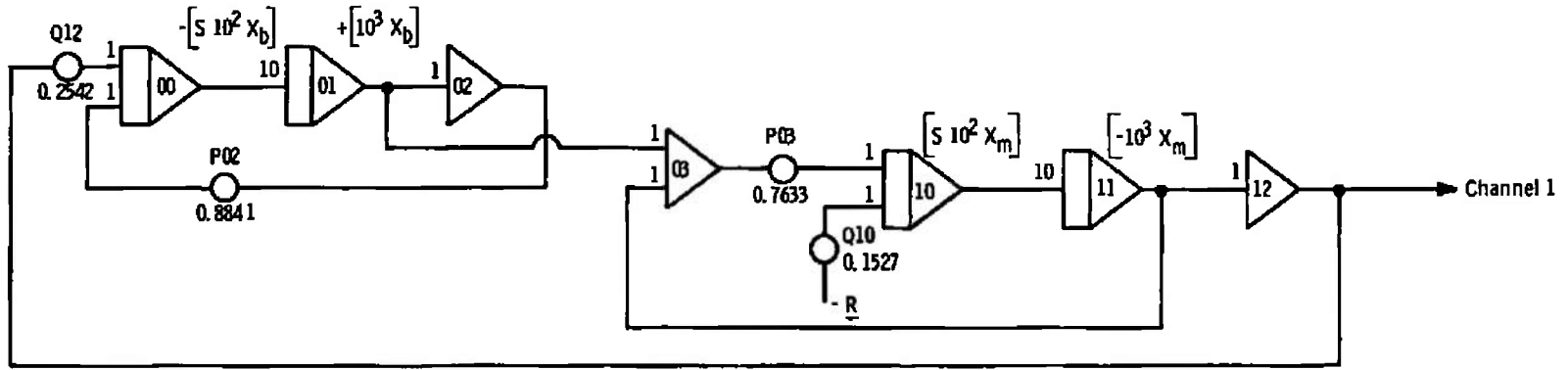
Equations (34), (35), and (36) were scaled and programed on the analog computer (Fig. III-1) for the case of a step change in  $T_m$  from zero to 20,000 lb. The system damping was also set to zero. Two undamped second-order systems were set up to produce  $10 \cos \omega_1 t$  and  $10 \cos \omega_2 t$  where  $\omega_1 = 2\pi(31)$  and  $\omega_2 = 2\pi(56.7)$ . The magnitude of  $A_1 + A_2$  was known since this corresponds to the steady-state value of  $X_m$  (0.028 in.) when the steady thrust is 20,000 lb. The sum of  $A_1 + A_2 - A_1 \cos \omega_1 t - A_2 \cos \omega_2 t$  (output of amplifier 24 in Fig. III-1-b) was observed on the repetitive operation display scope simultaneously with  $X_m$  from the stand simulation (output of amplifier 12, Fig. III-1-a). The coefficients  $K_1$  and  $K_2$  were manually varied until the two solutions coincided. The values for  $A_1$  and  $A_2$  were determined to be 22.75 and 5.25, respectively. Figure III-2 shows the responses of  $X_m$  and the general solution for these values of  $A_1$  and  $A_2$ . The cosine functions are plotted to show their values in relation to the response functions.

By experimenting with other frequency combinations it was determined that the low frequency shift can be predicted with the following equation:

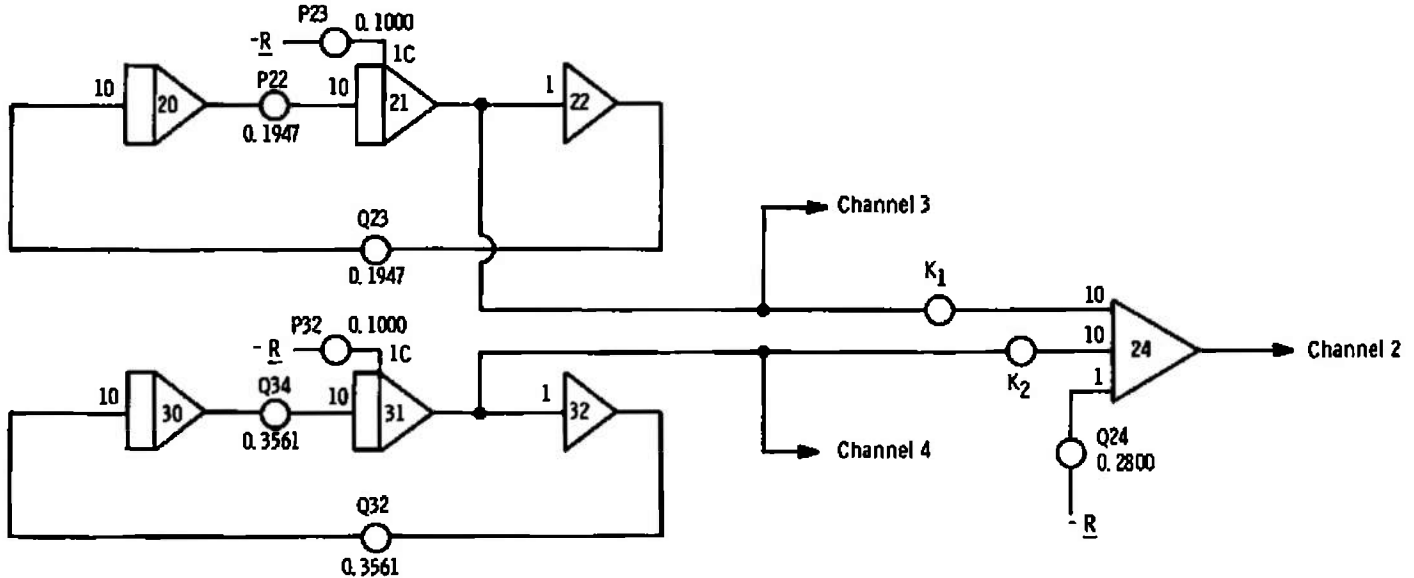
$$f = |af_1 - f_2|$$

where  $a = f_2/f_1$  rounded to the nearest integer.

In the above case  $a = 56.7/31 = 1.83$  and rounded becomes 2.0. The low frequency calculated using this criterion is 5.3 cps. This checks well with the observed frequency of 5.5 cps.



a. Simulation of Basic Undamped Thrust Stand



b. Circuit for Generating General Solution

Fig. III-1 Low Frequency Component Investigation

40

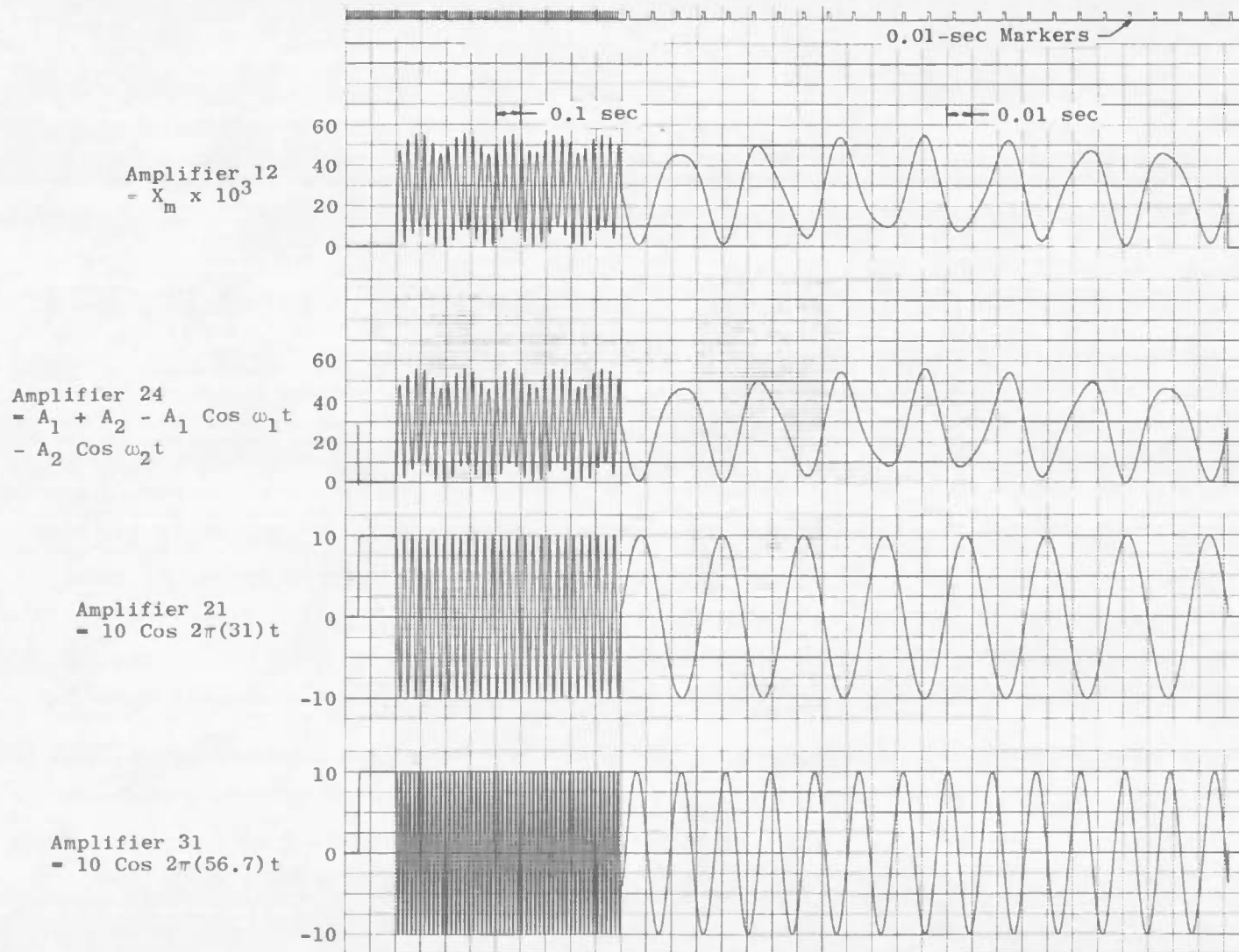


Fig. III-2 Data Recorded from the Computer Circuits of Fig. III-1

## DOCUMENT CONTROL DATA - R &amp; D

(Security classification of title, body of abstract and indexing annotation must be entered when the overall report is classified)

1. ORIGINATING ACTIVITY (Corporate author) Arnold Engineering Development Center ARO, Inc., Operating Contractor Arnold Air Force Station, Tennessee		2a. REPORT SECURITY CLASSIFICATION UNCLASSIFIED	
		2b. GROUP N/A	
3. REPORT TITLE ALTERATION OF THRUST STAND DYNAMICS USING HYDRAULIC FORCE FEEDBACK			
4. DESCRIPTIVE NOTES (Type of report and inclusive dates) Final Report May through August, 1967			
5. AUTHOR(S) (First name, middle initial, last name)  Sam P. Ragsdale, ARO, Inc.			
6. REPORT DATE December 1967	7a. TOTAL NO. OF PAGES 48	7b. NO. OF REFS 10	
8a. CONTRACT OR GRANT NO. AF 40(600)-1200	8a. ORIGINATOR'S REPORT NUMBER(S) AEDC-TR-67-232		
b. PROJECT NO. 5730	8b. OTHER REPORT NO(S) (Any other numbers that may be assigned this report) N/A		
c. Task 573004			
d. Program Element 6240518F			
10. DISTRIBUTION STATEMENT This document has been approved for public release and sale; its distribution is unlimited.			
11. SUPPLEMENTARY NOTES Available in DDC.		12. SPONSORING MILITARY ACTIVITY Arnold Engineering Development Center, Air Force Systems Command, Arnold Air Force Station, Tennessee	
13. ABSTRACT <p>This report is concerned with the dynamic behavior of a rocket motor and thrust stand combination when restrained by a hydraulic force balance system. The system is analyzed taking into account the nonlinearities caused by limiting flow and fluid compressibility. The analysis is followed by a discussion of the data obtained from an analog simulation of the system. Investigations of the basic stand without the servo are followed by investigations with the servosystem installed for comparison purposes. Both the time and frequency domains are investigated using ramp and sinusoidal forcing functions of thrust. The results of this investigation show that many desirable advantages may be realized using hydraulic force feedback. The control signals may be adjusted to provide zero displacement of the rocket motor position during the steady portion of the firing and at the same time, provide a high degree of damping. Concurrent with these conditions, the acceleration of the rocket motor may be greatly reduced during the firing transient.</p>			

14. KEY WORDS	LINK A		LINK B		LINK C	
	ROLE	WT	ROLE	WT	ROLE	WT
thrust stands rocket motors simulation hydraulic force balance servosystems						